SOME OPTO-ELECTRONIC COMPONENTS AND EXAMPLES OF THEIR APPLICATIONS

AV

H. HÅKANSON

DEPARTMENT
OF
SOLID STATE PHYSICS

INSTITUTIONEN FÖR FASTA TILLSTÅNDETS FYSIK
LUNDS TEKNISKA HÖGSKOLA-LUNDS UNIVERSITET
LUND-SWEDEN

1972

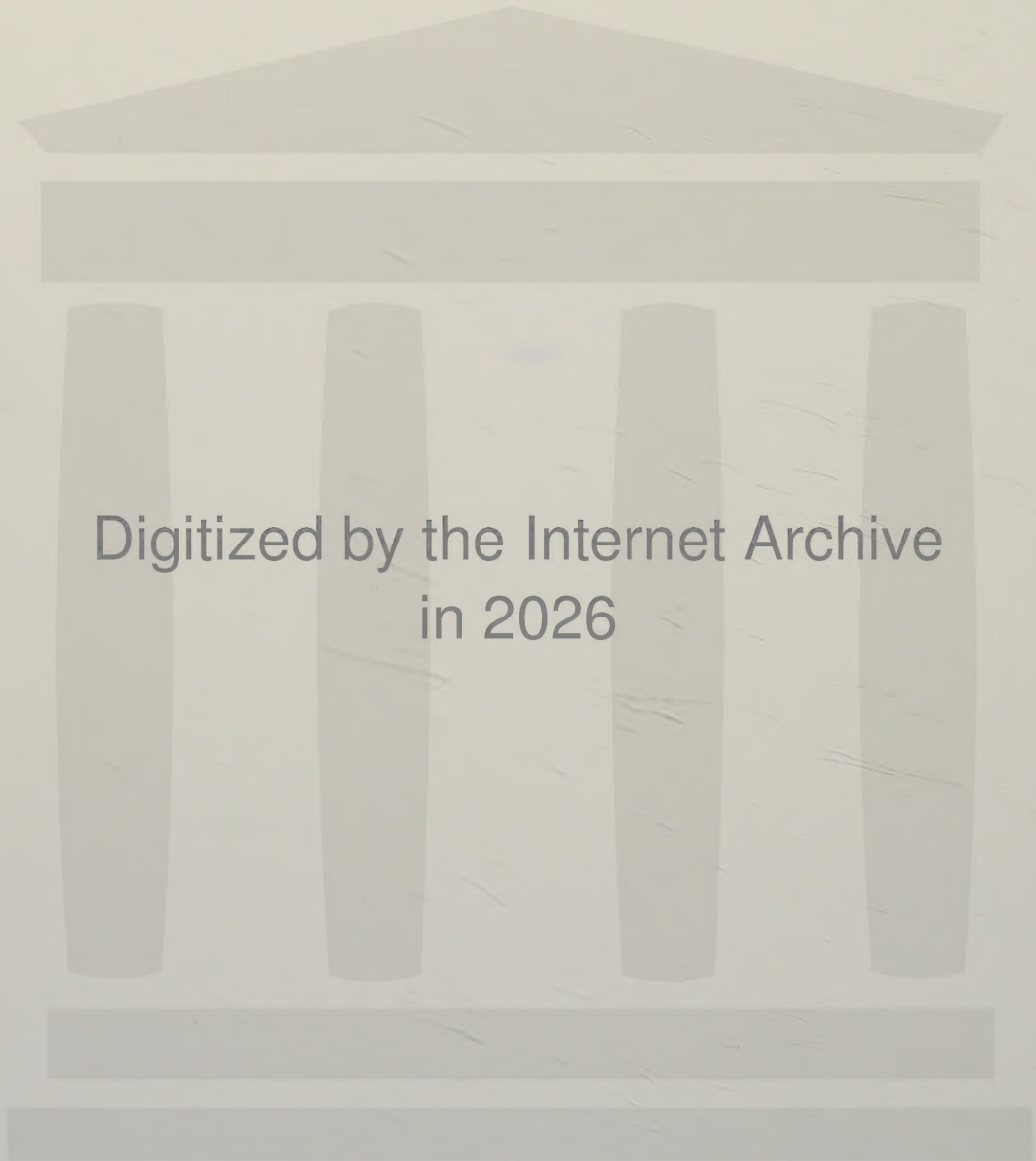
Digitized by the Internet Archive
in 2026

https://archive.org/details/IA41545326_0030

SOME OPTO-ELECTRONIC COMPONENTS AND EXAMPLES OF THEIR APPLICATIONS

AV

H. HÅKANSON

UNIV.
LEIDEN
BIBL.

Some opto-electronic components and examples of their applications.

H. Håkanson

Department of Solid State Physics,
Lund Institute of Technology, Box 725,
220 07 LUND, Sweden.

There are many types of opto-electronic components which nowadays are in use. The most common types are photo-diodes, photo-transistors, light emitting diodes and semiconductor lasers. During the last few years the number of types and applications have increased rapidly.

The purpose of this paper is to present a/ a new opto-electronic component [I], b/ an apparatus for determining the majority charge carrier type [II] and c/ to give some illustrations of opto-electronic applications [III, IV, V].

Some opto-electronic components and examples
of their applications.

B. Hök

Department of Solid State Physics,
Lund Institute of Technology, Box 725,
220 07 LUND, Sweden.

There are many types of opto-electronic components which nowadays are in use. The most common types are photo-diodes, photo-transistors, light emitting diodes and semiconductor lasers. During the last few years the number of types and applications have increased rapidly.

The purpose of this paper is to present a\ a new opto-electronic component [I], b\ an apparatus for determining the majority charge carrier type [II] and c\ to give some illustrations of opto-electronic applications [III, IV, V].

The present dissertation is based on the following papers:

I Capacity change with memory effect, accepted for publication in Electronic Engineering.

II Conductivity type determination for different semiconductor materials, The Review of Scientific Instruments, 43, 1380, 1972.

III Förbättring av metod för mätning av glans, preprint.

IV An opto-electronic system for determining thicknesses and diameters, preprint.

V A photometer for measuring short tracks of heavy nuclei stopping in nuclear emulsion, Cosmic Ray Physics Report, LUIP-CR-72 03, 1972, (together with L. Jacobsson and G. Jönsson).

The present dissertation is based on the following papers:

I Capacity change with memory effect, accepted for publication in Electronic Engineering.

II Conductivity type determination for different semiconductor materials, The Review of Scientific Instruments, 43, 1380, 1972.

III Förbättring av metod för mätning av plana, preprint.

IV An opto-electronic system for determining thickness and diameter, preprint.

V A photometer for measuring short tracks of heavy nuclei stopping in nuclear emulsion, Cosmic Ray Physics Report, LUIP-CR-72 03, 1972, (together with L. Jacobsson and G. Jönsson).

The component presented in the first paper [I] is a diode, the capacity of which can be varied by optical means. What distinguishes the present device from a normal photo-diode is that it has a memory effect [1] due to the presence of deep levels. In our case we use an epitaxial gold-doped silicon diode [2], but the same effect is found in copper- or oxygen-doped gallium phosphide [1,3]. The mechanism of the memory effect is explained according to reference 1 and two applications are given. The first application is a direct method for using the capacity change as an opto-electronic transmission with a built-in memory. The capacity of the diode determines the resonance frequency of a LC-oscillator, the change in the output frequency being proportional to the change in capacity. In the second application the component is an integral part of a voltage divider [4]. The resolution in this circuit can be made very high. Other possibilities of utilizing the device are as a light integrator or as an optical memory for the storage of binary-coded signals.

The determination of majority charge carrier type is often a very difficult problem, especially when, as is the case for many types of photo-diodes, epitaxial layers are involved. A system has been developed which makes it rather easy to determine the conductivity type [II]. The properties of several semiconductor materials of known resistivities have been checked and the method has been found to be both reproducible and

reliable. The determination takes no longer than some seconds and the minimum size of sample which can be handled is 1,5 x 0,5 mm. The surface of the crystal must be carefully cleaned but no etching is needed.

Care must be taken in the choice of a light emitting source and detector for an opto-electronic system, the matching of spectral response being particularly critical. When other optical components such as lenses and mirrors are included in a system, it is important to know the photon energy dependence of both the transmission and reflectivity [5]. The improvement made possible by proper selection of the light emitter and detector for an opto-electronic system is shown in paper [III].

One of the great advantages of opto-electronic systems is the lack of mechanical contact with the sample under investigation, which means that the system has a long lifetime and can be used in rough environments. In paper [IV] an example of such a system which is also adapted for automatic data processing is given.

The properties of the system are determined not only by the opto-electronic component, but also by the surrounding electronic system. In paper [V] a photometer for measuring track width in nuclear emulsions

is described. The electronic system is designed for high linearity and accuracy [6]. G. Jönsson et al [7,8] have earlier presented a similar system and also described the results of tests of the complete system.

Acknowledgements

I wish to express my most sincere thanks to Professor H.G. Grimmeiss for his support, stimulating guidance and never-failing interest during this work. My sincere thanks are also due to Professor S. Berglund for his guidance during my studies in electronics.

To Egon Persson, Jens Henriksen, Hans Ljungquist and Peter Johansson I would like to express my gratitude for their expert assistance in the mechanical build up of my experiments.

My sincere thanks are due to Mrs Ingrid Hammar and Miss Eva Johansson for their kind help in typing my manuscripts.

Finally I would like to thank all my colleagues in the Department of Solid State Physics and Institute of Physics for their valuable help and good comrade-ship.

References:

1. Grimmeiss, H.G., Olofsson, G., Journal of Applied Physics, 40, 2526, 1969.

2. Sah, C.T., Forbes, L., Rosier, L.L., Tasch, JR, A.F., Solid-State Electronics, 13, 759, 1970.

3. Björklund, G., Grimmeiss, H.G., Solid-State Electronics, 14, 589, 1971.

4. Foldvari, T.L., Lion, S., Instruments & Control Systems, 37, 77, 1964.

5. Moses, A.J., Optical Materials Properties, Handbook of Electronic Materials, Vol 1, 1971.

6. Håkanson, H., Erlandsson, B., Nuclear Instruments & Methods, 70, 205, 1969.

7. Jönsson, G., Kristiansson, K., Malmqvist, L., Cosmic Ray Report No K.S. 6903, 1969.

8. Jönsson, G., Kristiansson, K., Malmqvist, L., Astrophys and Space Sci, 7, 231, 1970.

Capacitance change with memory effect

H Håkansson

Department of Solid State Physics, The Lund Institute of Technology, Box 725, S-220 07 Lund 7, Sweden

When the space-charge region of a p-n junction is changed the capacitance of the junction is also changed. The width of the transition region depends on the space-charge density which can be altered either by an applied voltage or by illumination. The purpose of this paper is to show two applications utilizing the possibility of controlling the capacitance by illumination.

The diode which is used in these applications is a gold-doped p^+-n silicon diode. Figure 1 shows the energy band diagram and the charge density respectively before the diode is doped with gold. As can be seen from the figure the p-side is heavily doped (10^{18} cm^{-3}) and the n-side has about $5 \cdot 10^{15}$ charge carriers per cm^3.

After doping the situation shown in figure 2 is found. Gold causes two impurity centres in silicon, one donor level and one acceptor level. The ratio of the photo-ionization cross sections of these levels is such that the donor level can be neglected in this case if extrinsic light is used |1, 2, 3|.

In thermal equilibrium at room temperature, the gold acceptor centres under the Fermi level E_F are occupied and the centres above E_F unoccupied. The width of the space-charge region is now increased compared with that of the undoped diode. Illumination changes the population ratio of the centres. The energy, E_o, required to fill the gold centres is higher than that to make them empty, E_e. The centres therefore are emptied when illuminated with light of low energy (figure 3). The situation is similar to that before doping and the width W_2 of the space-charge region is smaller than W_1. Light of high energy will increase the population ratio of filled states. The maximum amount (80 %) is achieved at a photon energy of 1.15 eV |1|. From figure 4 we can see that the width W_3 is increased.

Since the space-charge region has very few free charge carriers compared with the regions on both sides, we can regard the capacitance of the junction as that of a parallel-plate condenser, the capacitance of which is given by $C = \frac{\varepsilon \varepsilon_o A}{W}$

where ε = the dielectric constant of the material

ε_o = the dielectric constant of free air

A = the junction area

W = the width of the space-charge region.

If the junction is illuminated with light of higher energy than E_e but lower than E_o, the capacitance of the junction is increased. On the other hand the capacitance will decrease if the energy of the applied light is higher than E_o but lower than the bandgap E_g, since the gold level is occupied. When the junction is

illuminated with light of higher energy than that of the bandgap, holes will be injected and the centres emptied because we illuminate from the n-side. This results in the same situation as if we had used light of low energy.

At low temperatures (for this diode under 150 K), the thermal excitation can be neglected. This means that there will be no change in the population ratio after the illumination is stopped. This is a memory effect |4|. The intensity of the applied light determines the speed of the capacitance change. Figure 5 shows the construction of the diode.

Two applications with the diode as an opto-electronic component have been investigated. The first is an optically-tuned oscillator and the second an optically-variable potentiometer.

Optically-tuned oscillator

The block diagram of the circuit is shown in figure 6. The capacitance of the diode is included in the frequency-determining LC-circuit. Since the capacitance of the diode is as low as approximately 60 pF the stray capacitances can cause problems by reducing the ratio $\frac{\Delta C}{C}$, where ΔC is the difference in capacitance between the states where the diode is illuminated with ligth of energies 1.15 eV and 1.8 eV light. Measurements of the ΔC as a function of back-bias show |1| (figure 7) that there is only a slight dependence. However, the capacitance of the diode decreases rather much when the back-bias of the diode is increased.

The complete oscillator circuit is shown in figure 8. Since the capacitance of the diode is rather low, it is not practical to design an oscillator for low frequencies. The low frequency range is included by mixing with another fixed oscillator.

The maximum variation in frequency attained with this circuit is 60 kHz, which can be increased by reducing the stray capacitances, increasing the oscillator frequency or by putting a large back-biassing voltage on the diode.

Optically-tuned potentiometer

The circuit used in this case is shown in figure 9 |5,6|. The variations in capacitance of the diode used as a condenser are utilized.

The ac-generator which can supply either sine or square waves, charge Cd in the positive half of the period and C2 in the negative. During the period when the diode D2 is back-biassed, C2 is discharged through R2 in series with the parallel coupling of R1 and Rℓ. In the same manner, Cd is discharged through R1 in series with the parallel coupling of R2 and R1 when D1 is reversed-biassed. When Cd is equal to C2, the average output signal across R1 during one period is zero. When C2 is different from Cd, the output voltage is an alternating current superimposed on a dc-signal. The dc-signal is measured. With the following assumptions, the theoretical output signal V is given by equation 1 |5,6|.

1. $R1 = R2 = R$

2. The dc-level over the diode is such that the diode is back-biassed during the whole period (figure 11).

$$V = Vi\ R\ell\ \frac{R + 2R\ell}{(R + R\ell)^2}\ R\ f\ (Cd - C2 - Cd\ e^{-k_1} + C2\ e^{-k_2}) \quad (1)$$

where $k_1 = \frac{R + R\ell}{2R\ f\ Cd(R+2R\ell)}$ and $k_2 = \frac{R + R\ell}{2R\ f\ C2(R+2R\ell)}$, f is the frequency of the generator and Vi is the source voltage.

From the equation, it is seen that the output voltage and the change in capacitance of the diode are not linearly related. However, if k_1 and k_2 are large, the deviation from a linear dependence becomes small. High sensibility can only be obtained at the expence of the linearity. The frequency-dependence of the circuit is shown in figure 10. As can be seen, the frequency-dependence is small and there are no problems with the frequency stability of the source. The amplitude stability of the generator is critical (figure 12) and a well-stabilized generator is needed.

A very important factor in dealing with potentiometers is their resolution, i e the minimum shift in resistance ΔR divided with the total resistance R. If the potentiometer is used as a voltage divider, the ratio $\frac{\Delta R}{R}$ is equal to $\frac{\Delta V}{V}$ where ΔV is the minimum detectable voltage change and V is the voltage across the potentiometer. The resolution is limited by the noise voltage generated across the resistances ($V_{noise} = \sqrt{4\ kTBR}$) and flicker in supply voltage. In this particular case, it is possible to reduce the noise by decreasing the values of the resistances and then adjusting the frequency so that the same sensibility is achieved.

V is limited by the maximum output voltage of the generator.

In the application described here with an ac-generator (Rodhe Schwartz) ΔV is 0.1 mV and V is 200 mV which gives $\frac{\Delta V}{V} = 5 \cdot 10^{-4}$. This ratio can be improved by a factor 5 if a generator with better stability is available. It is also possible to increase the ratio $\frac{\Delta V}{V}$ by increasing the voltage V. The diode can stand 100 V in the reverse direction and in this case the output voltage would have been 1 V, giving an improvement by about a factor of 5. This corresponds to $\frac{\Delta V}{V} \simeq 2 \cdot 10^{-5}$. Since the mechanism of the capacitance changing effect is known, it is possible to increase ΔC and consequently $\frac{\Delta V}{V}$. There is no theoretical limit for the ratio $\frac{\Delta C}{C}$. The resolution found here is about the same as that of a normal precision potentiometer (typically $2 \cdot 10^{-4}$). With the modifications described above, the resolution for this circuit becomes $\simeq 2 \cdot 10^{-5}$ which is a considerable improvement.

Common to this application and a usual potentiometer is that both systems have common zero level. This would not be the case if a bridge was used. Very important advantages of this circuit are the high isolation resistance and the lack of mechanical contact, which will result in a longer lifetime and the possibility of use in rough environments.

Another feature of this circuit is that it can be used as an light integrator (figure 13).

In materials with higher bandgap which show the same kind of memory effect |4|, there is no need for cooling which makes the device more attractive to the constructor.

Acknowledgements

The author owes sincere thanks to Professor H G Grimmeiss for helpful discussions and stimulating interest during the performance of this work. I am also grateful to S Braun for very valuable discussions.

References

1. S Braun, H G Grimmeiss, to be published

2. C T Sah, L Forbes, L L Rosier and A F Tasch,Jr, Solid State Electronics 13, 759 (1970)

3. C T Sah, V G K Reddi, IEEE transaction on Electron Devices, 11, 345 (1964)

4. H G Grimmeiss, G Olofsson, Journal of Applied Physics, 40, 2526 (1969)

5. T L Foldvari, S Lion, Instruments & Control Systems 37, 77 (1964)

6. K S Lion, The Review of Scientific Instruments 33, 353 (1964)

Component list

T1, T2, T3	Transistor MPS 918 Motorola	
Z1	Zenerdiode BZY C5V1 Siemens	
C1	Variable capacitor 3-30 pF	
C2	Ceramic capacitor 82 pF	
C3, C4	Ceramic capacitor 5000 pF	
R1	Resistor 15 k	
R2	" 3,9 k	
R3	" 10 M	
R4	" 3,3 k	
R5	" 1,2 k	
R6	" 1,0 k	all carbon 5 %, 1/4 W
R7	" 150 k	
R8	" 39 k	
R9	" 1,0 k	
R10	" 0,1 k	
R11	" 3,9 k	

Figure captions

Figure 1 The energy band diagram and the charge density before the diode is doped.

Figure 2 The energy band diagram and the charge density after doping with gold.

Figure 3 The energy band diagram and the charge density when the centres are emptied.

Figure 4 The energy band diagram and the charge density when the centres are filled.

Figure 5 The construction of the diode.

Figure 6 Block diagram of the optically-tuned oscillator.

Figure 7 Variations of ΔC, C and $\Delta C/C$ as a function of back-bias.

Figure 8 Complete oscillator circuit.

Figure 9 Circuit of the optically-tuned potentiometer.

Figure 10 The output voltage as a function of generator frequency.

Figure 11 The input voltage Vi (5V/cm) and the voltages across Cd and C2 (2V/cm) as a function of time (5μs/cm).

Figure 12 The output voltage as a function of generator voltage.

Figure 13 The output voltage as a function of applied light intensity and time.

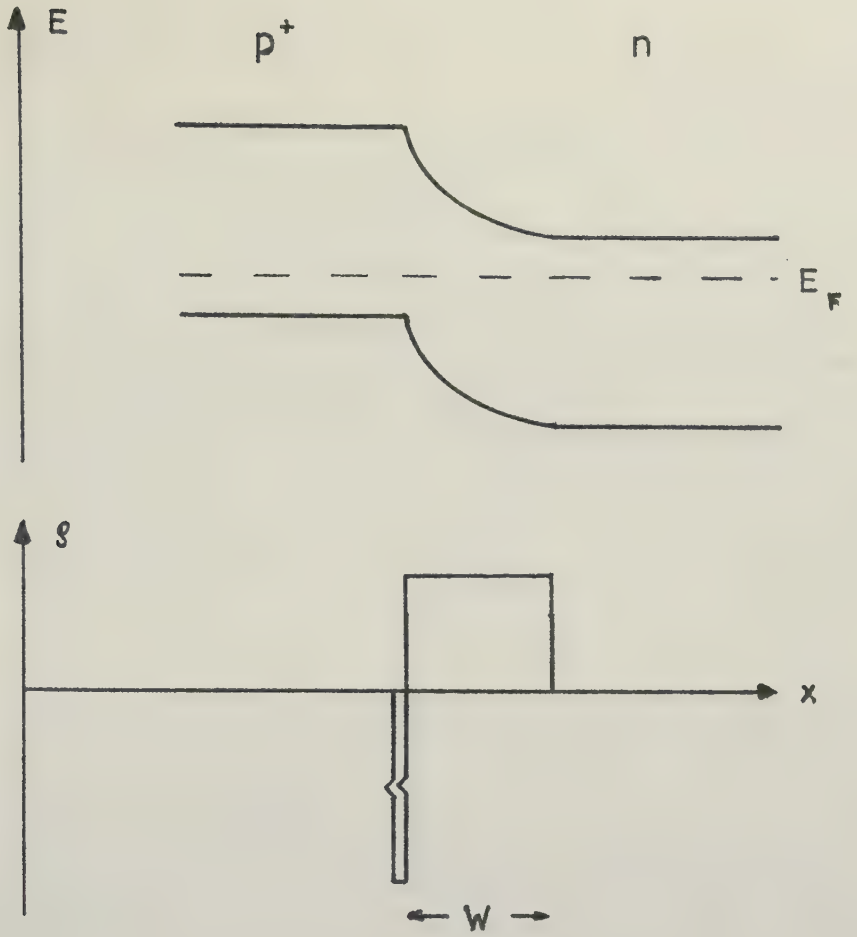

Figure 1

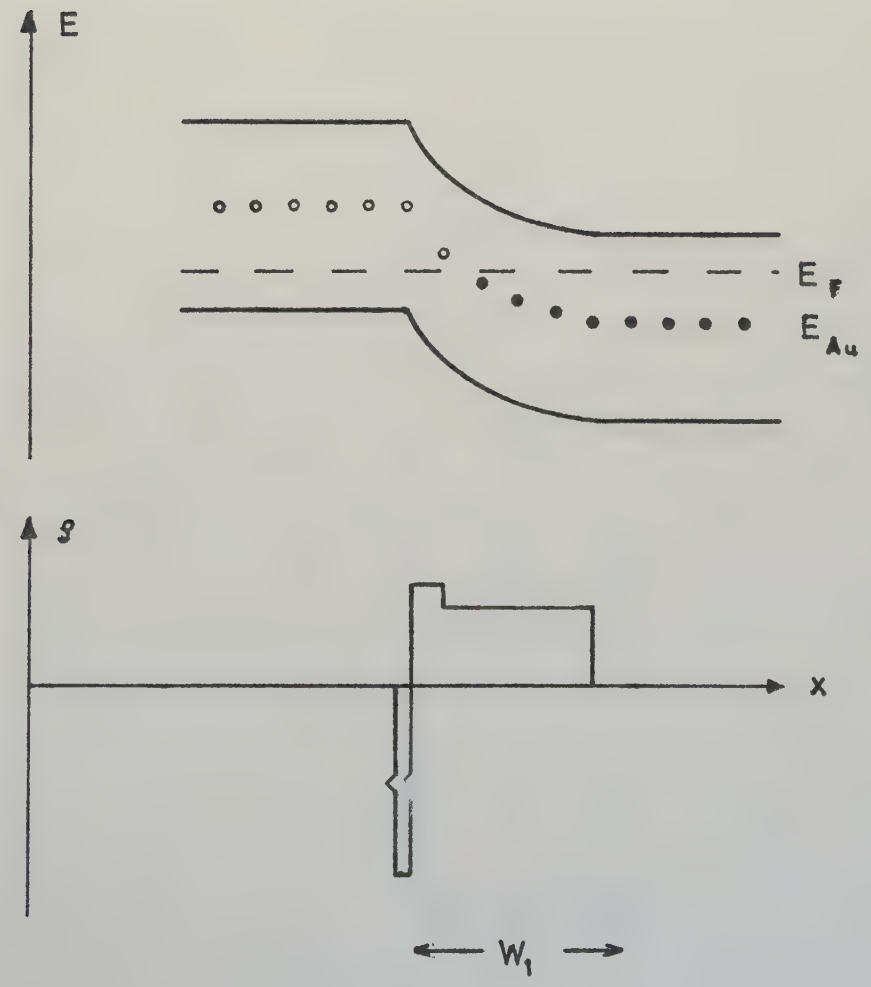

Figure 2

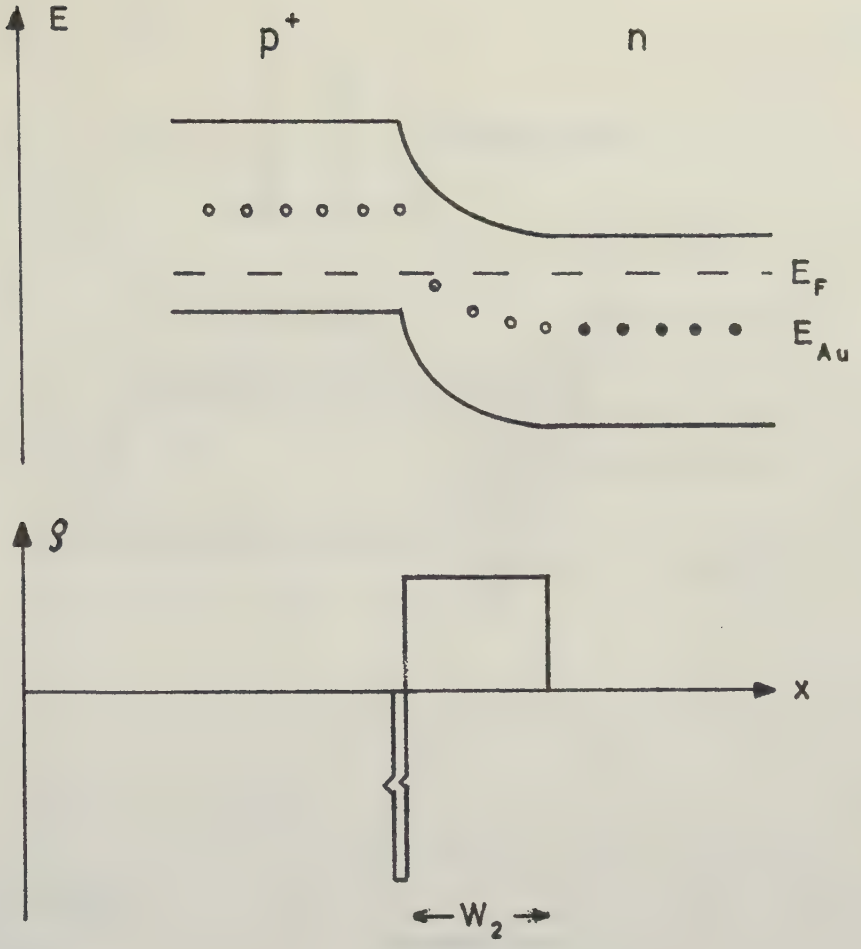

Figure 3

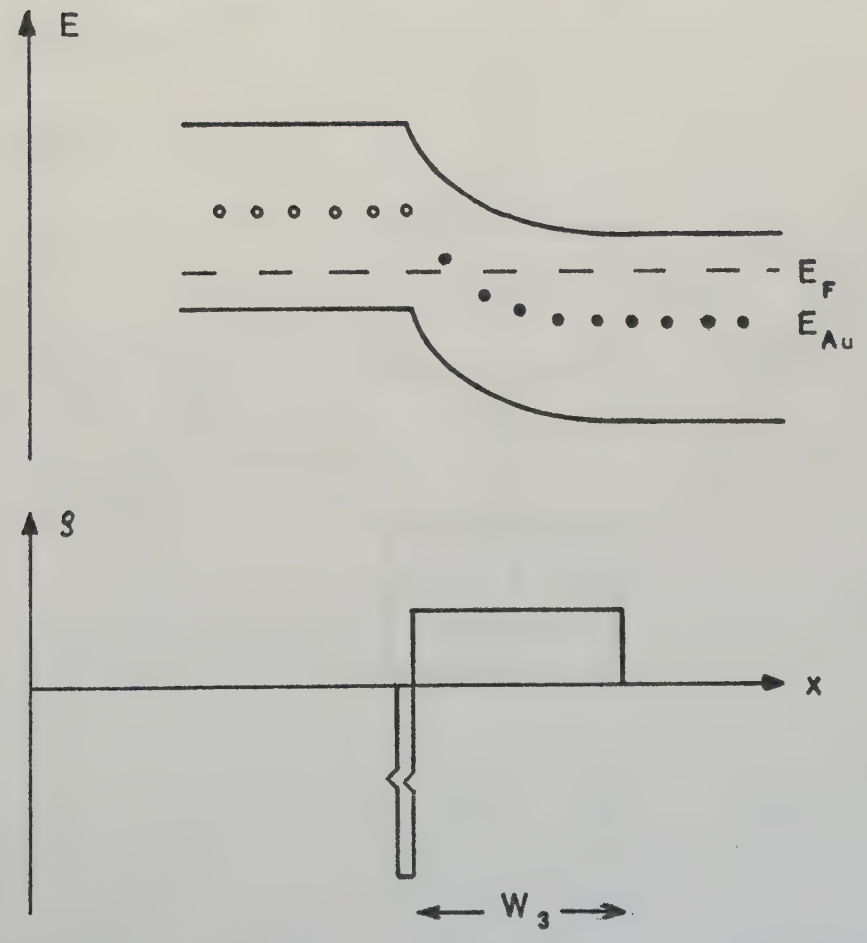

Figure 4

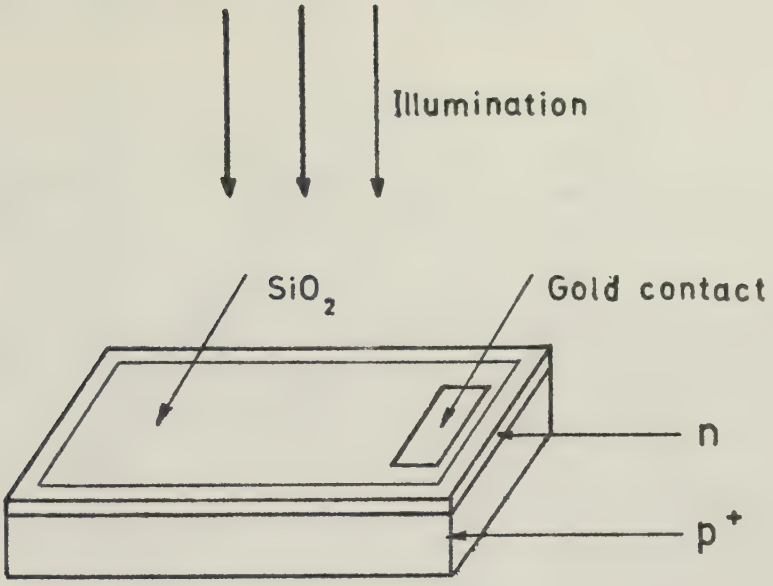

Figure 5

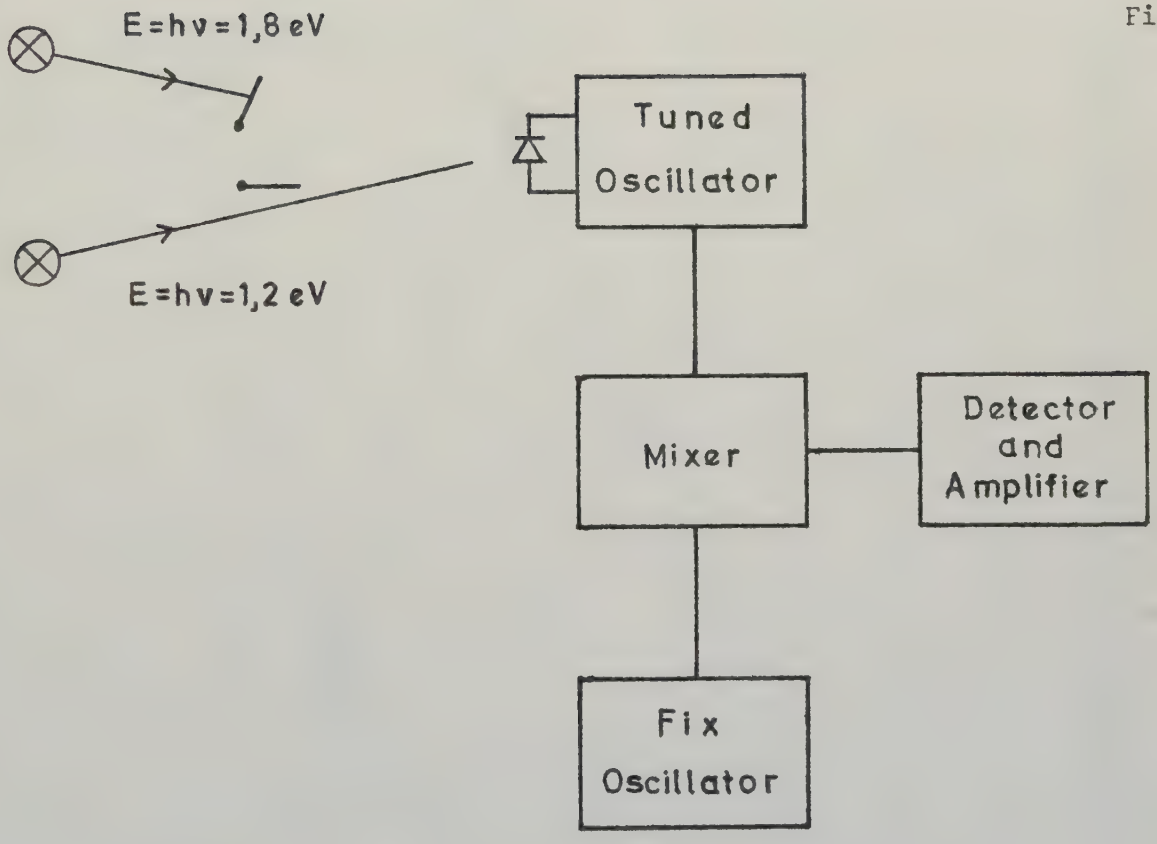

Figure 6

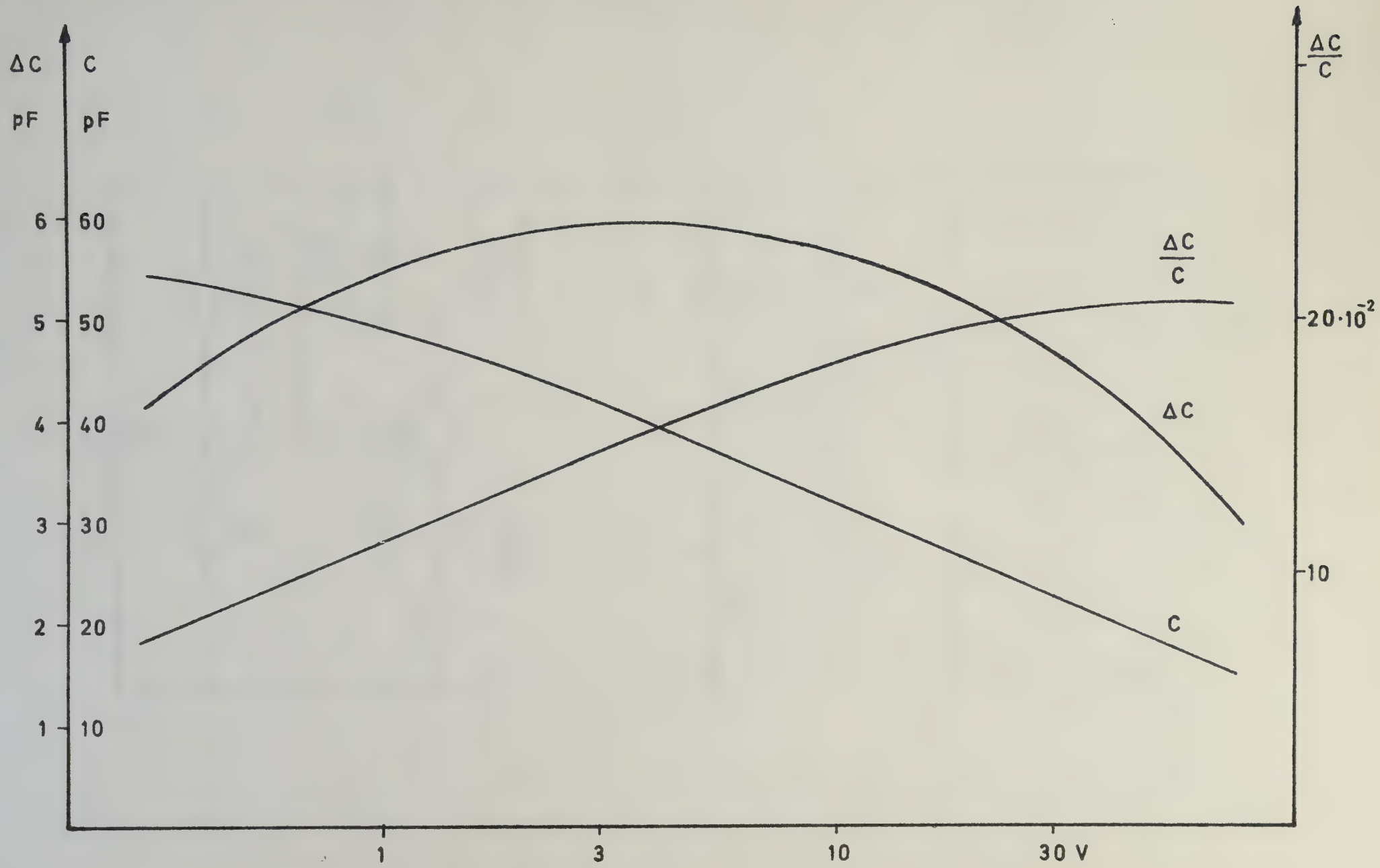

Figure 7

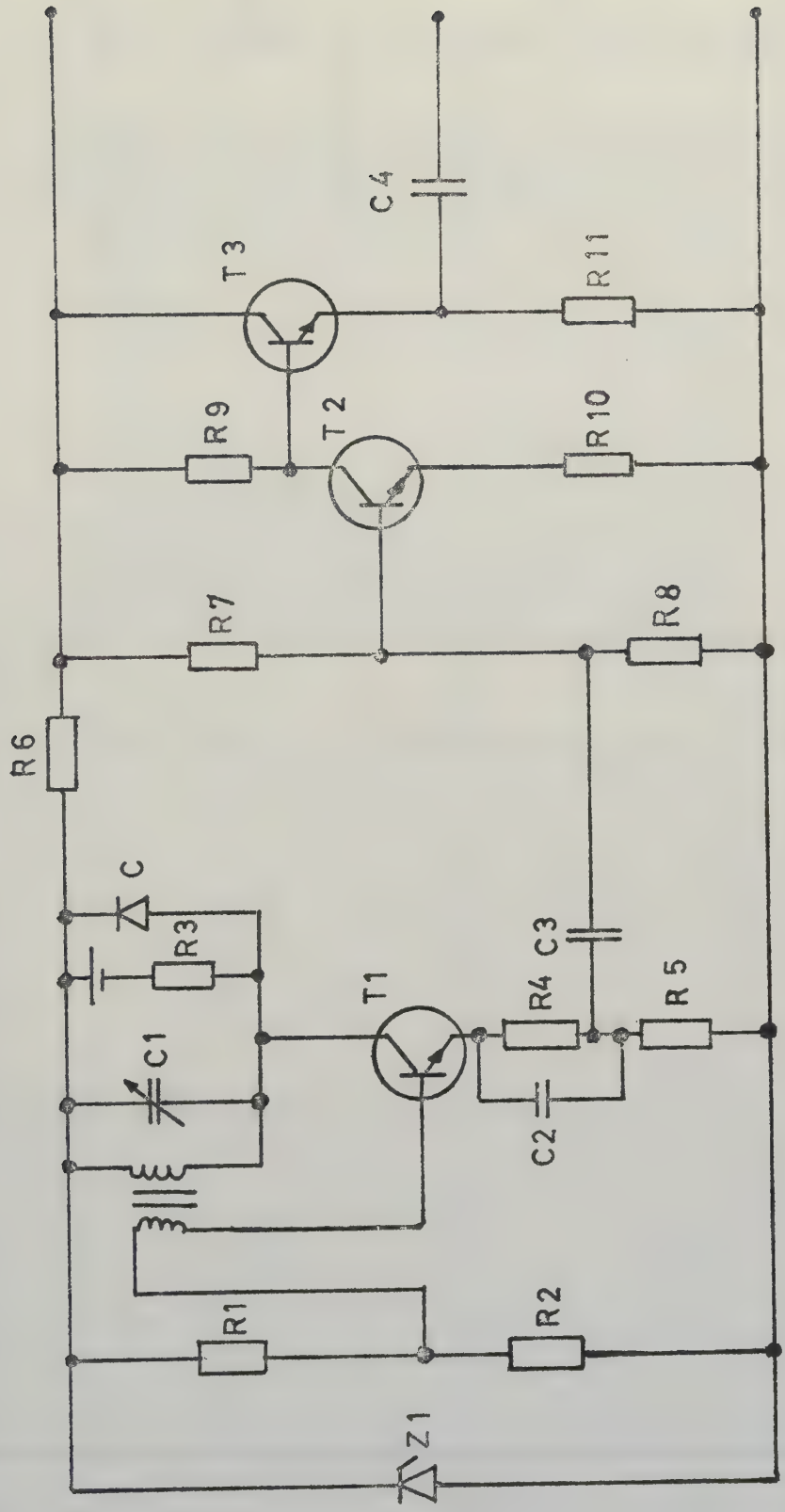

Figure 8

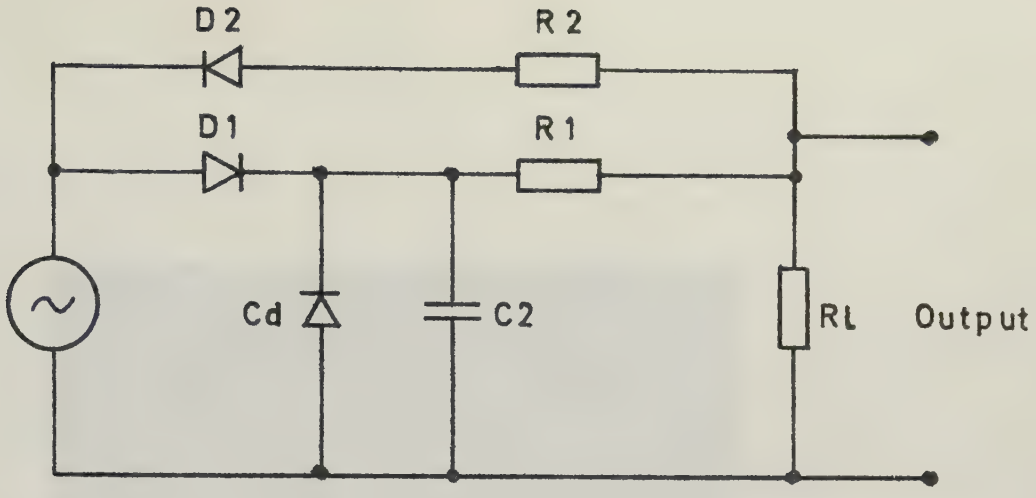

Figure 9

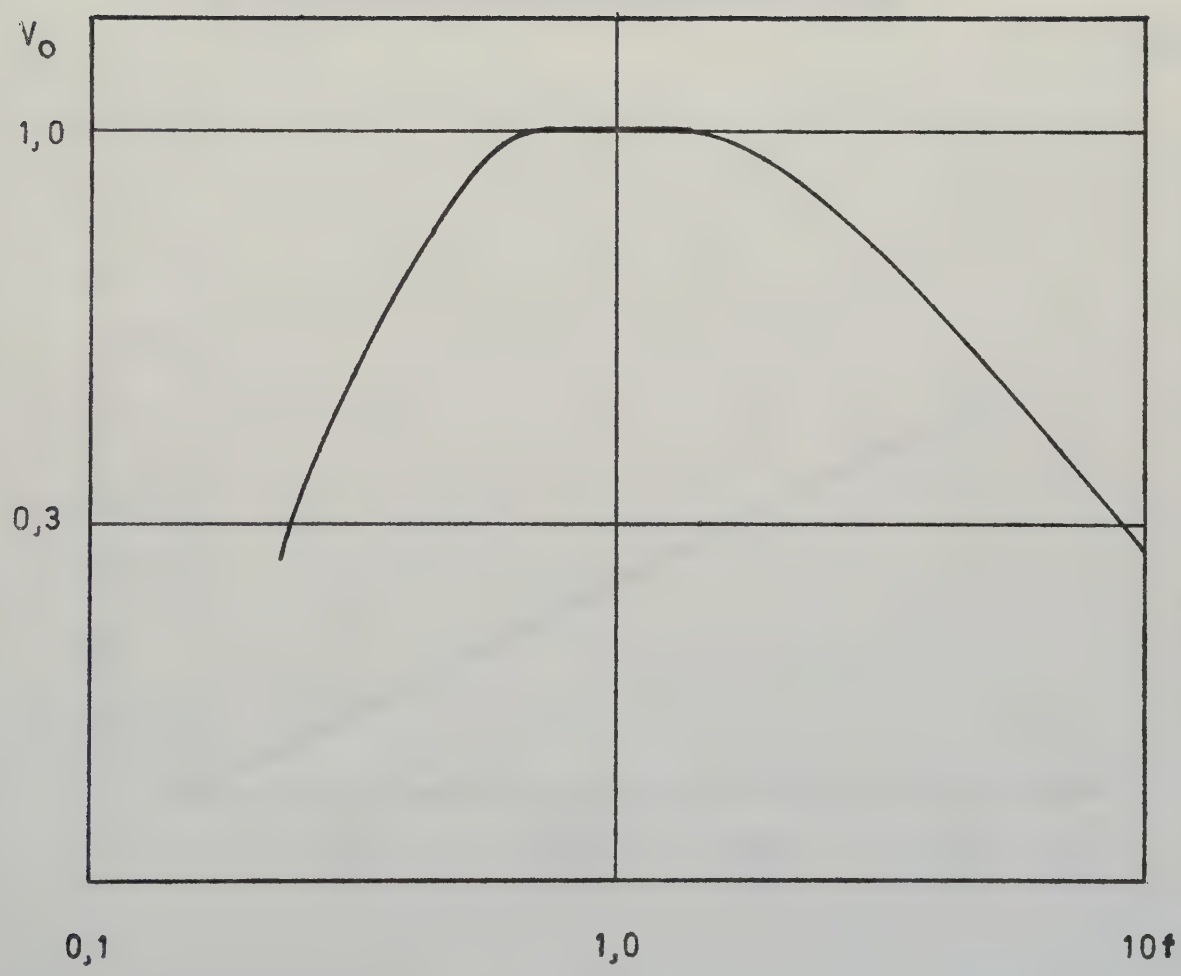

Figure 10

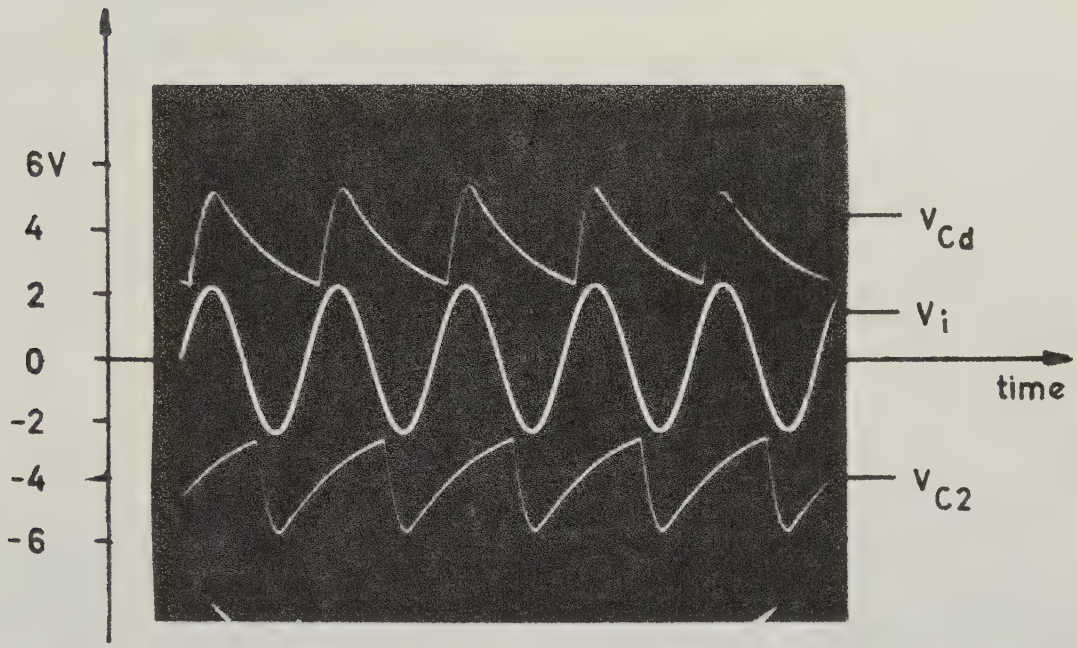

Figure 11

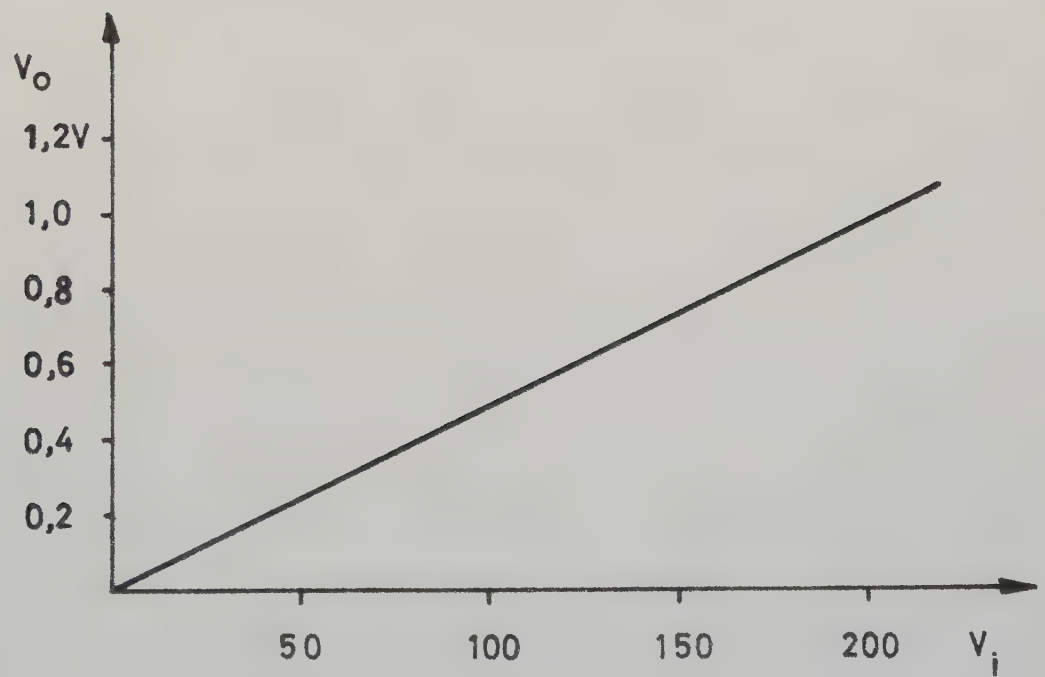

Figure 12

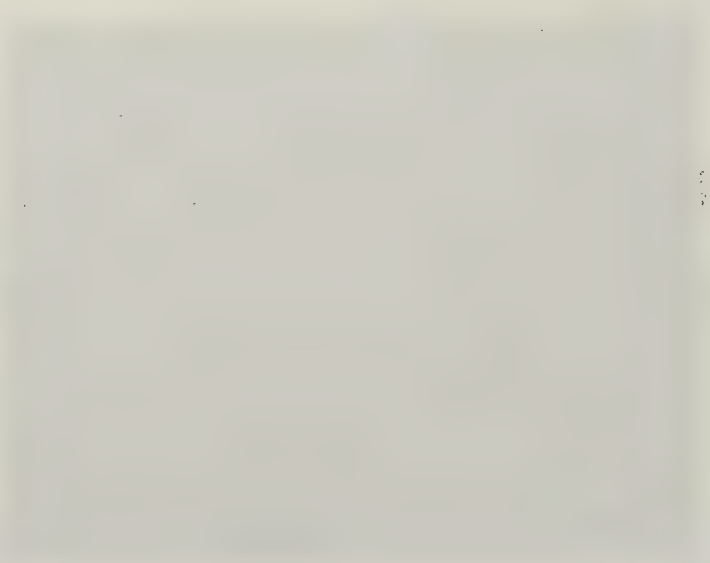

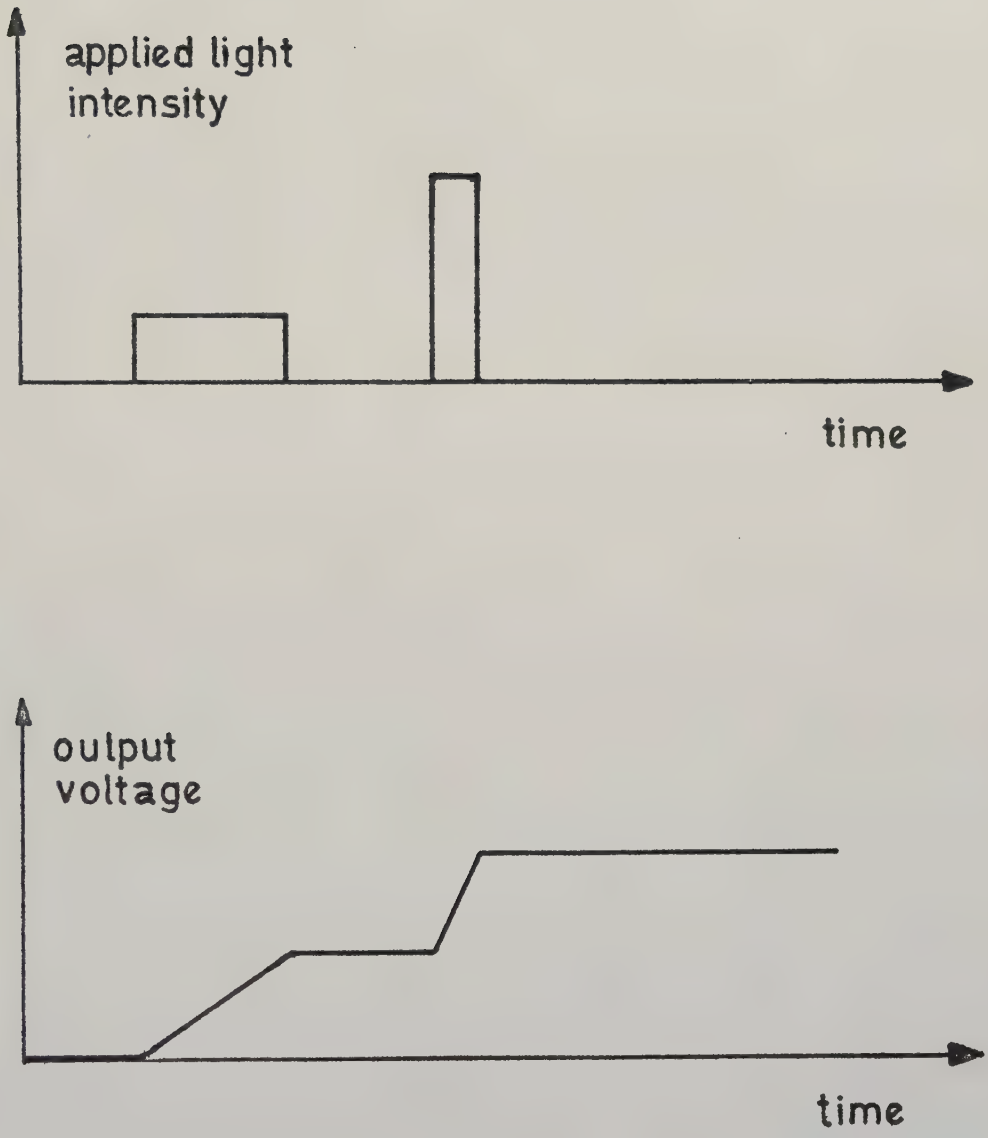

Figure 13

CONDUCTIVITY TYPE DETERMINATION FOR DIFFERENT SEMICONDUCTOR MATERIALS

Håkan Håkanson

Department of Solid State Physics, The Lund Institute of Technology, L u n d, Sweden

There are several methods of determining the conductivity type using e g the Hall effect, the photovoltaic effect, the thermoelectric effect or the rectifying effect. Each method has both advantages and drawbacks. In the particular case of epitaxial layers, the best choice appears to be using rectification and the thermoelectric effect.

The purpose of this paper is therefore to present a system for the determination of the conductivity type utilizing rectifying contacts and the thermoelectric effect. Furthermore the results which have been achieved in this way for different materials will be given.

The system used is similar to that described by Kean, Schneider and Pillus [1]. The experimental set-up is shown in figure 1.

Let us assume that the rectifying contact will be forward biassed when the metal contact has higher potential than the

semiconductor (see figure 2). The equivalent circuit for a rectifying contact can in this case be represented by an ideal rectifier and in parallel a resistor the magnitude of which is determined by the leakage current when the rectifying contact is reverse biassed. The voltage drop over the ideal rectifyer is neglected and the resistances in the sample between the contacts are denoted by r1 and r2.

During the half period when contact D1 is forward biassed the equivalent circuit can be reduced to that in figure 3. The output voltage V_{out} will follow the input voltage V_{gen} and the output amplitude will be determined by V_{gen} and the magnitude of the resistances. From figure 3, it follows that

$$V_{out} = \frac{V_{gen}\, R}{\left[\dfrac{r1}{\dfrac{R2(r2+R3+R)}{R2+R3+r2+R}} + 1\right](R+r2+R3)} \qquad (1)$$

If R2, R3 $\gg$ r1 and r2 which is true in most applications, equation (1) becomes

$$V_{out} = \frac{V_{gen}\, R}{R3 + R} \qquad (2)$$

The output voltage will decrease if the input impedance (R) of the voltmeter is less than R2 and R3. It is therefore desirable to use a high input impedance voltmeter. The shape of the input and output voltages is shown in figure 4.

During the other half period, D2 and D3 act as short

circuits and the equivalent circuit becomes that in figure 5. From the figure it is clear that the output voltage will be zero during this period. As the net result over one or more periods we get a positive output voltage. Should the rectifying contacts be forward biassed when the metal has lower potential than the semiconductor, we would get a negative output voltage. The polarity of the rectifying contacts for a metal to n-type semiconductors is opposite to the polarity of the metal to p-type semiconductors [1-4]. It is therefore possible to determine the conductivity type by observing the polarity of the output voltage. If the contacts are rectifying, the current from the generator will be very small. But if the contacts are ohmic or if there is breakdown in the material, the current will be large and the determination of the carrier type uncertain. To be able to separate rectifying from non-rectifying contacts, a current measuring instrument is placed in series with the generator.

For our measurements we used a Fell probe for making the point contacts. The radius of the tips is $4 \cdot 10^{-2}$ mm and the pressure on each contact is $25 \cdot 10^{-3}$kg. If we assume that the pressure is spread over half the surface area we deduce a pressure of approximately 10 kg/mm^2. This is sufficiently large for the probe to be able to penetrate thin oxide layers. If the pressure is too high the surface might be damaged, see figure 6, or the crystal broken. This can be avoided if a proper choice of substrate is used.

INDICATING INSTRUMENT

The indicating system is shown in figure 7. An operational amplifier with field effect-transistor input (Teledyne Philbrick 1009) is used. The input impedance is determined by the resistor R5 and is in our application 10^8 ohms. The voltage gain A is equal to R4/R3 and is here chosen to be about 20. A smoothing capacitor C1 is placed in parallel with the feedback resistor. The indicating instrument has centre zero and is protected against overload by R1, D1 and D2.

RESULTS

In the case of silicon, 12 samples in the resistivity range from 0.14 ohm-cm to $6 \cdot 10^4$ ohm-cm have been tested. In all cases the correct type of conductivity compared with that given by the manufacturer has been found. Some of the samples have also been tested by the thermoelectric effect and these results were in agreement with those obtained from rectification measurements.

In studying gallium arsenide we had 16 samples in the resistivity range from $3 \cdot 10^{-3}$ ohm-cm to $7 \cdot 10^{+7}$ ohm-cm which also showed the correct type compared with data given by the manufacturer. Only for one sample with a resistivity of $1.4 \cdot 10^8$ ohm-cm did the indicator indicate n-type in contradiction to that given by the manufacturer. Some of the samples in the low resistivity range could also be tested with the thermoelectric effect and consistent results were obtained. Four germanium samples with resistivities of 3-4 ohm-cm gave the correct type as well as

4.5 ohm-cm gallium phosphide (2 samples) and gallium nitride (3 samples).

DISCUSSION

Some difficulties can appear when very pure semiconductor materials are used. This is presumably because even very small amounts of impurities will cause a change in majority charge carrier type. When dealing with pure materials it is important to have a very clean surface. To achieve this the surfaces have been polished so that the maximum size of the unevenesses is approximately 1 μm. After polishing the sample is cleaned in pure tricloroethylene then pure acetone and finally distilled water [5].

This method of using rectifying contacts has also been utilized to detect the location of p-n junctions in crystals. In this case the material is polished into a wedge-shaped form and the location of the junction is where the conductivity changes from one type to another.

A great advantage for this method over others is that the measurements can be done very rapidly.

By a very slight modification the system allows those of the samples which have breakdown for low voltages or make poor rectifying contacts to be determined using the thermoelectric effect (see figure 8).

ACKNOWLEDGEMENTS

The author owes sincere thanks to Professor H G Grimmeiss for helpful discussions and stimulating interest during the performance of this work.

The test materials were kindly supplied by L Å Ledebo.

REFERENCES

1. W A Keenan, C P Schneider, C A Pillus, Type-All System for Determining Semiconductor Conductivity Type, Solid State Technology March 1971, p 51

2. H K Henisch, Rectifying Semiconductor Contacts, Oxford, 1957

3. A Many, Y Goldstein, N B Grover, Semiconductor Surfaces, North-Holland Publ Co, 1965

4. D Geist, Halbleiterphysik, Sperrschichten und Randschichten, F Vieweg & Sohn, Braunschweig, 1970

5. D R Frankl, Electrical Properties of Semiconductor Surfaces, Pergamon Press 1967

FIGURE CAPTIONS

Figure 1 The test set-up utilizing rectifying contacts.

Figure 2 The equivalent circuit for figure 1.

Figure 3 During the half period when contact D1 is forward biassed the equivalent circuit can be reduced.

Figure 4 The generator and output voltages as a function of time.

Figure 5 The reduced equivalent circuit when contact D1 is reverse biassed.

Figure 6 A gallium arsenide surface which has been damaged by the probe tip.

Figure 7 Complete circuit of the indicating instrument.

Figure 8 The test set-up utilizing the thermoelectric effect.

COMPONENT LIST TO FIGURE 7

Q1	1009 Operational amplifier Teledyne Philbrick
D1, D2	3× 1N914 Diode Texas Instrument
R1	4.7 kohm 5% 1/4 W Carbon
R2	1 kohm 5% 1/4 W Carbon
R3	10 kohm 5% 1/4 W Carbon
R4	220 kohm 5% 1/4 W Carbon
R5	100 Mohm 5% 1/4 W Carbon
C1	5000 pF 10% Ceramic

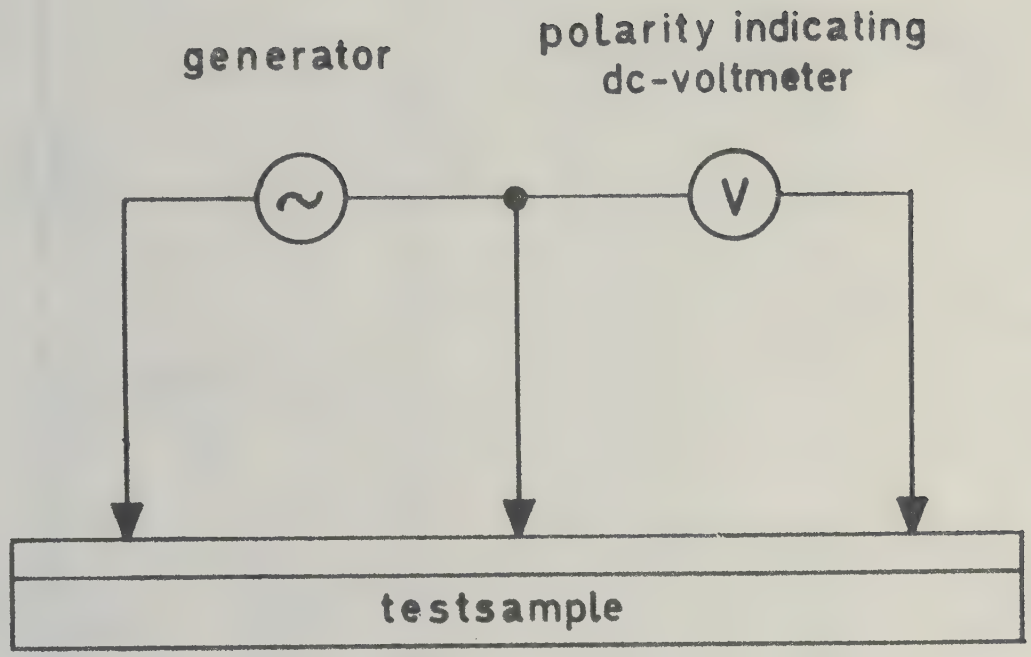

Figure 1.

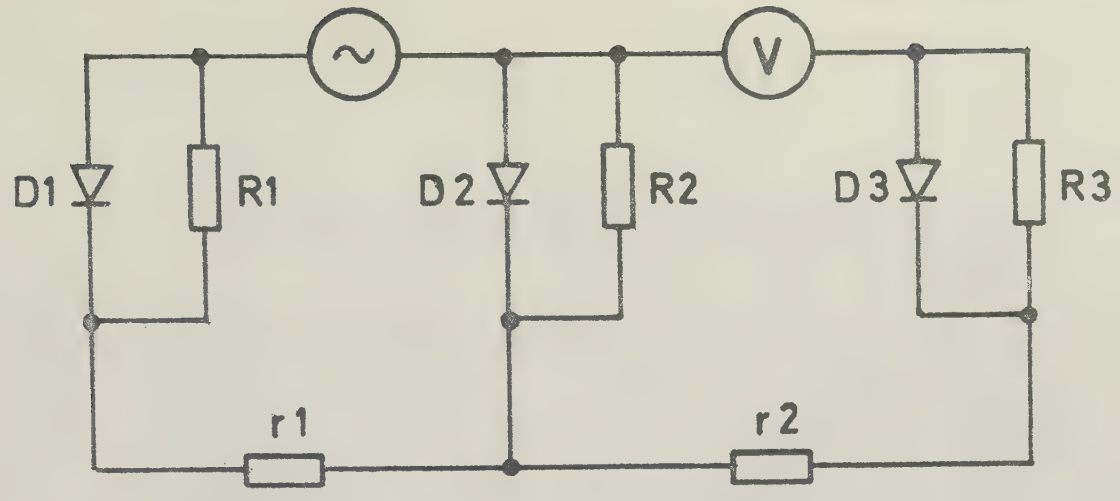

Figure 2.

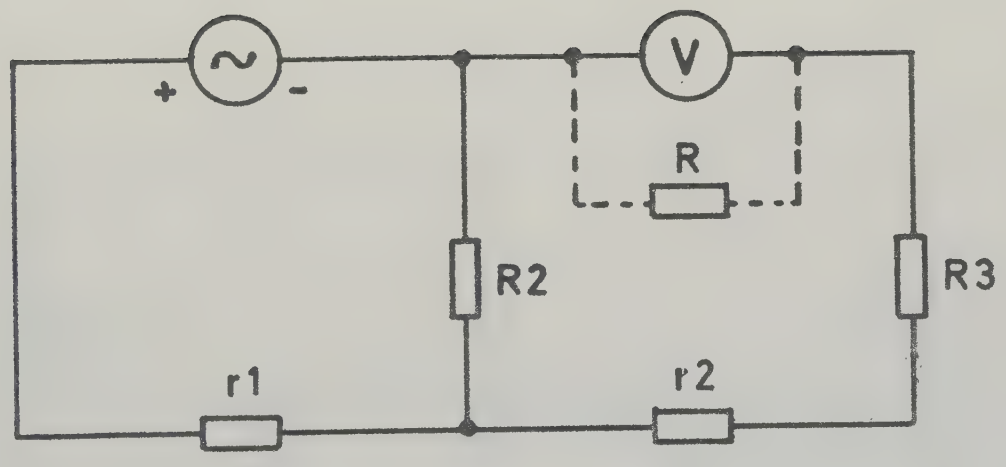

Figure 3.

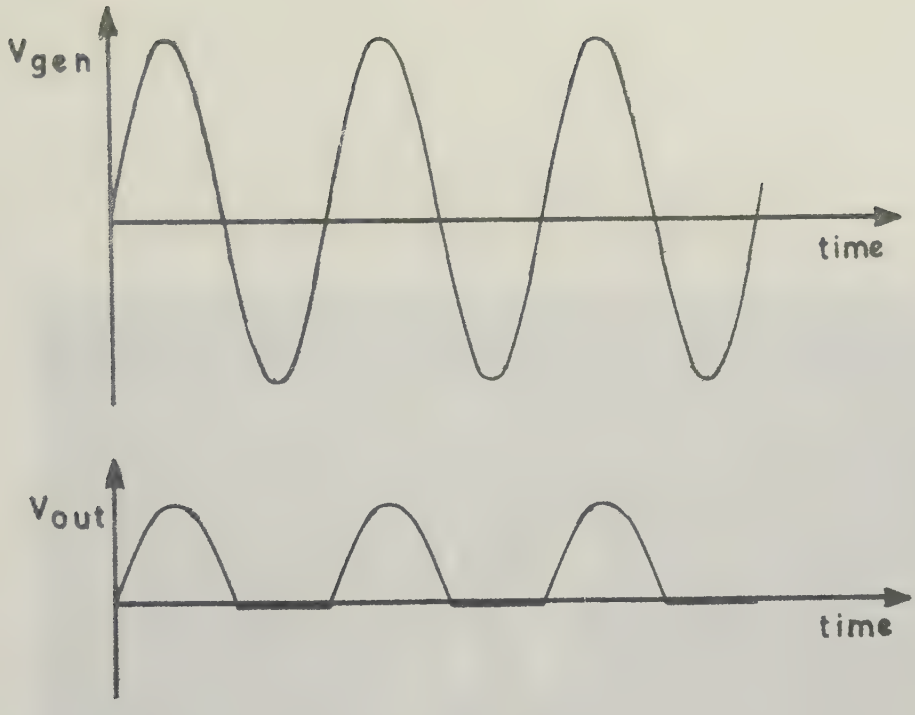

Figure 4.

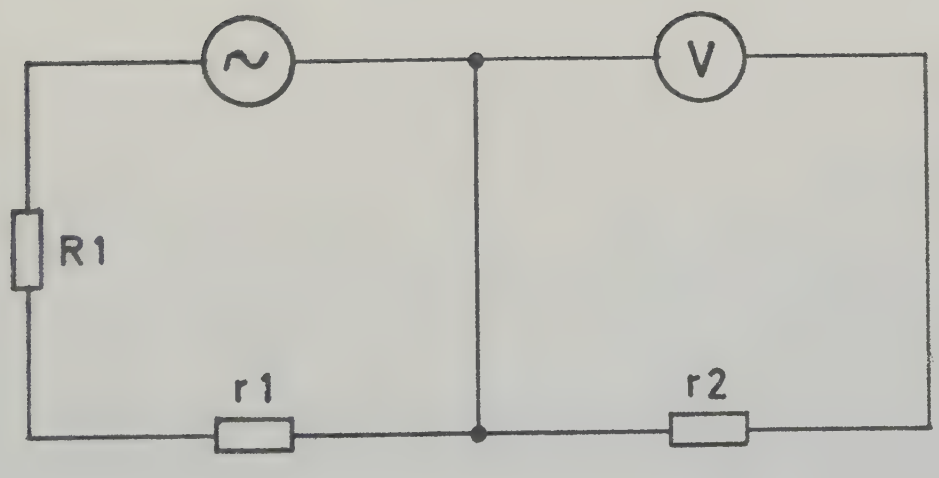

Figure 5.

Figure 6

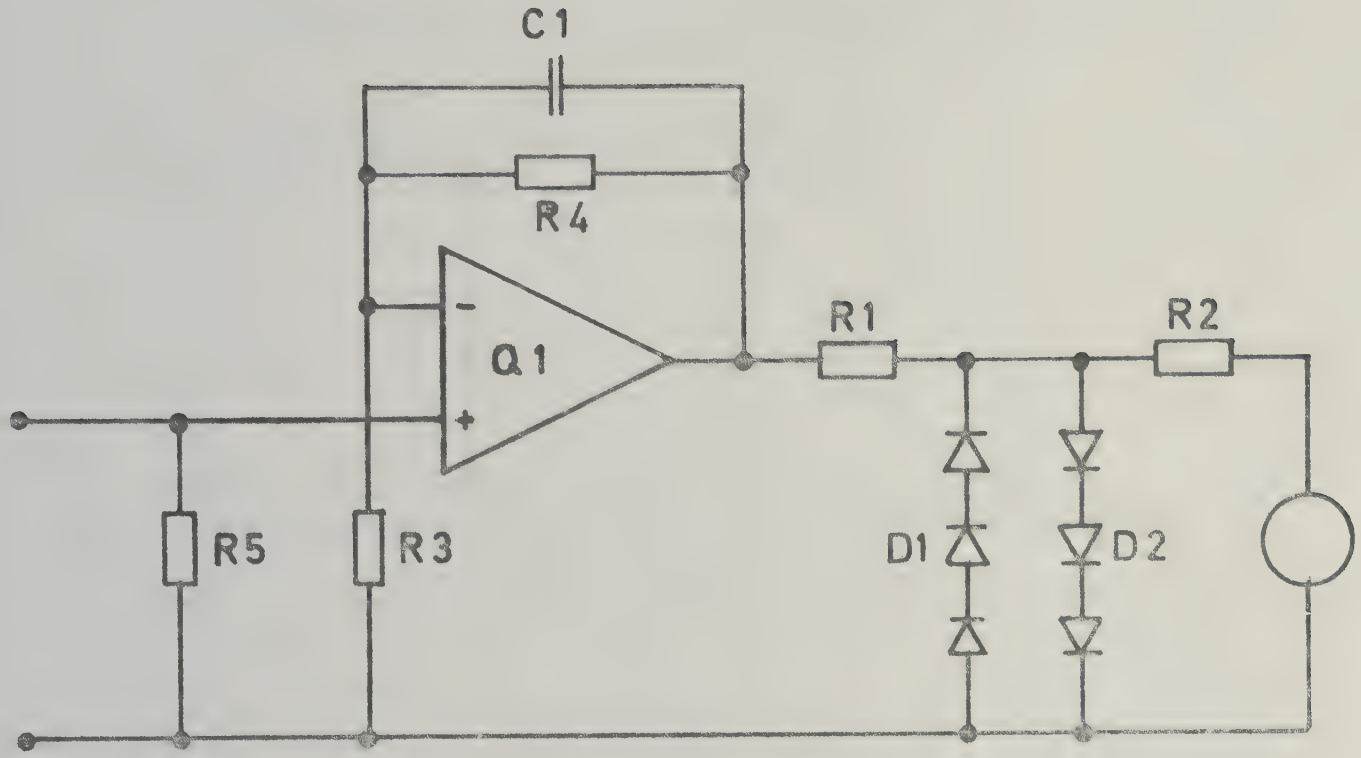

Figure 7.

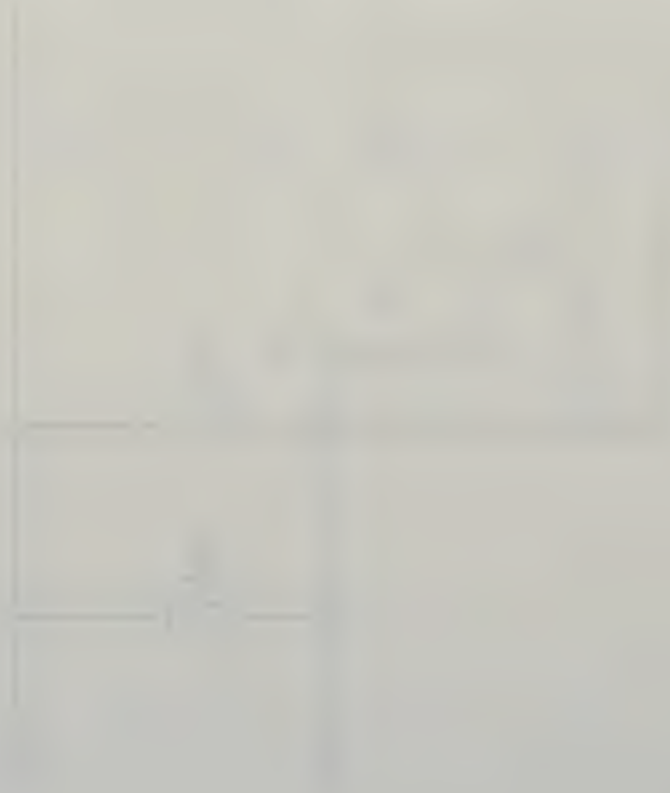

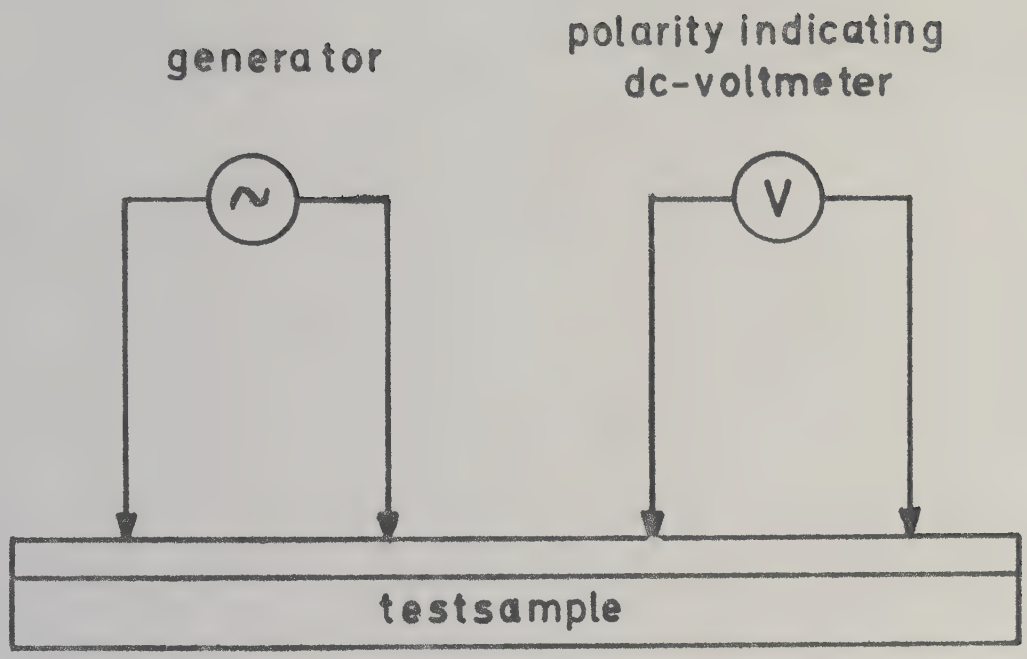

Figure 8.

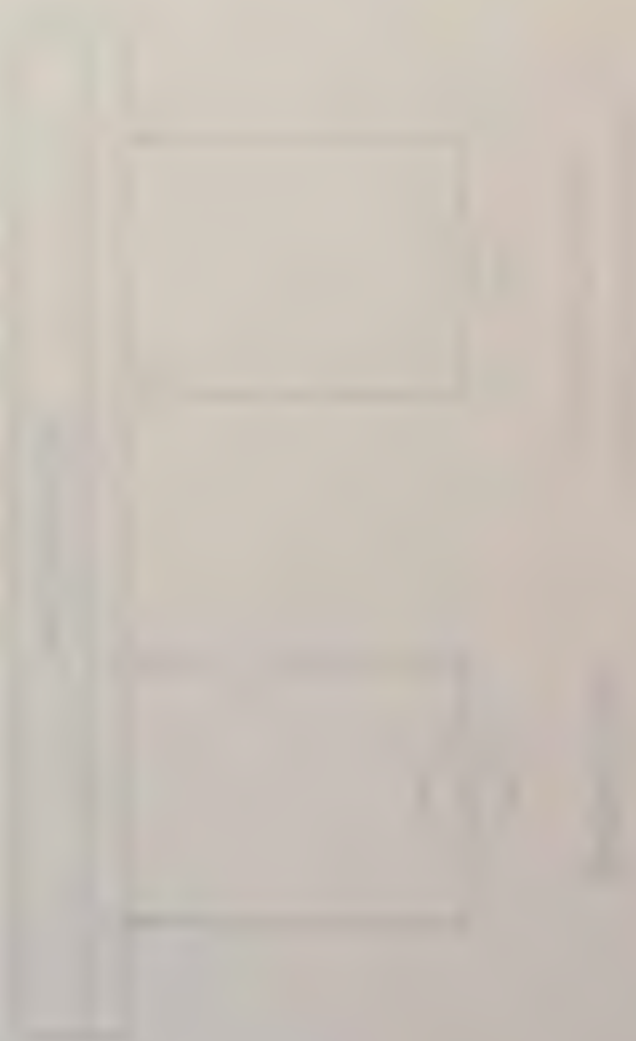

Förbättring av metod för mätning av glans hos bearbetade ytor.

Håkan Håkanson

Institutionen för fasta tillståndets fysik

Lunds Tekniska Högskola

Det är önskvärt att kunna mäta graden av bearbetning hos olika metallytor. Som mått användes glans. Med glans hos en yta menas dess förmåga att reflektera infallande ljus. Reflekteras allt ljus säges den vara spegelblank, sprides däremot ljuset kraftigt kallas den matt. Avsikten med detta papper är att visa hur en glansmätare kan förbättras genom lämpligt val av ljuskälla och detektor.

En bearbetad yta är behäftad med ojämnheter vars avvikelser i förhållande till medelytan kan anges som den aritmetiska medelavvikelsen Ra (figur 1) som ges av: $Ra = \frac{1}{L}\int_0^L y\,dx$. Man kan också ange den kvadratiska medelytavvikelsen Rs som definieras som: $Rs = \sqrt{\frac{1}{L}\int_0^L y^2\,dx}$. För slipade och polerade ytor som i allmänhet uppfyller kravet på stokastisk fördelning kan man emellertid genom mätningar visa att Ra-värdena och Rs-värdena varierar på samma sätt. Detta betyder att man inte har någon större variation av lutningsvinklarna för olika bearbetningsförfaranden så länge man inte ändrar Ra eller Rs värdena.

Glansen kan bland annat mätas på två olika sätt:

1. Studium av ytans förmåga att avbilda ett objekt.

2. Studium av det reflekterade och spridda ljusets intensitetsfördelning.

Den första metoden kan endast användas på ytor med hög ytjämnhet och är dessutom en subjektiv mätning. Den andra metoden kan mäta ytor med stora variationer i ytnoggrannhet. Metoden är också objektiv vilket gör den mera tillförlitlig. Det praktiska utförandet av den senare metoden kan ske på flera olika sätt:

a. Intensiteten hos det reflekterade ljuset studeras som funktion av reflektionsvinkeln Θ. Den erhållna kurvan kallas goniofotometerkurva (figur 2,3). Halvvärdesbredden på det direkt reflekterade ljuset tages som mått på ytnoggrannheten dvs glansen.

b. Intensiteten hos det direkt refleterade ljuset jämföres med det för en spegelblank referensyta. I detta fall kan glansen G definieras som $G = \frac{R}{R_{ref}}$.

c. I reflektionsvinkeln Θ_R mätes intensiteten R av det direkt reflekterade ljuset. Vidare mätes intensiteten i en riktning som endast ger det spridda ljuset D (figur 4). Definitionen av glansen blir i detta fall: $G = \frac{R}{D}$.

d. Glansen kan också bestämmas genom mätning av endast det direkt reflekterade ljuset och G blir i detta fall lika med $\frac{1}{D}$.

e. Ytterligare en metod är att låta aperturvinklarna vara olika och på det sättet mäta intensiteten dels på det direkt reflekterade ljuset plus det spridda ljuset dels på endast det direkt reflekterade ljuset (figur 5). Som mått på glansen får vi $G = \frac{R}{R+D}$.

Kravet på mätmetoden är att den skall ge ett mått på yt-

noggrannheten antingen korrelerat till den aritmetiska ytmedelavvikelsen Ra eller den kvadratiska ytmedelavvikelsen Rs.

Den metod som experimentellt ger bäst korrelation mellan ytavvikelse och mätutslag är den under punkt e beskrivna. Denna princip utnyttjas i glansmätaren 8510-1 från C E Johansson och det är denna mätare som undersökningen avser att förbättra. Genom kvotmätningsförfarandet påverkas denna glansmätares utslag mindre av krökning hos mätytan än vad är fallet för de metoder som endast mäter reflekterat ljus (referens 1-3). Det praktiska utförandet av det optiska systemet för kvotmätningsförfarandet visas i figur 6, referens 7. Principen för mätaren är att ljuskällans strålknippe göres parallellt och får sedan träffa provytan under cirka 45 graders infallsvinkel. Genom att ha olika stora aperturvinklar mäter detektor 1 och 2 det direkt reflekterade respektive det direkt reflekterade plus det diffust reflekterade ljuset. Som detektor användes kadmiumsulfid motstånd vars resistivitet inom ett visst område är direkt proportionellt mot belysningens intensitet (referens 8). Ljuskällan är en glödlampa med volframglödtråd. Innan glansmätningen påbörjas kalibreras mätaren så att fullt skalutslag erhålles för en spegelblank yta.

Strömvariationer i glödlampan eller glödtrådens åldring medför inte bara variationer i intensitet utan även förskjutning av spektralfördelningen. Som visas i figur 7 är överlappningsområdet mellan emissionskurvan för glödlampan och känsligheten hos CdS-motståndet mycket litet. Områdets storlek ändras också markant då emissionskurvan förskjutes.

Detta medför att glansmätaren måste omkalibreras vid varje förändring av strömmen genom ljuskällan.

Av de teorier som studerats framgår det viktiga faktum att våglängden på det infallande ljuset påverkar förhållandet mellan det direkt reflekterade och det spridda ljuset, referens 3-7. Detta framgår också av de experimentella mätningar på olika provytor som företagits. Figur 8 visar försöksuppställningen och resultaten visas i figur 9 och 10. Anledningen till reflektionens våglängdsberoende är bland annat absorption i undersöksmaterialet. Absorptionen är olika för skilda material (referens 9). Sker ingen omkalibrering kan mätmetoden ge felaktigt samband mellan ytavvikelse och utslag.

Genom att överlappningsområdet ligger på glödlampans emissions exponentiella svans medför en förändring av lampströmmen en mycket stor förändring i resistiviteten hos CdS-motståndet. Användes som ljuskälla i stället en GaAsP diod (FLV 100) kommer CdS-motståndets resistivitet inte längre att påverkas lika mycket av strömmen genom ljuskällan. Anledningen till detta framgår dels av figur 7 som visar diodens spektralfördelning dels av det faktum att det emitterade ljusets intensitet är direkt proportionellt mot diodströmmen. Förändringen i spektralfördelning då strömmen varieras är i detta fall försumbar. Ännu bättre hade en laserljuskälla varit men kravet på en transportabel utrustning kan då inte längre uppfyllas.

Känslighetsmaximum för kadmiumsulfidmotståndet ligger vid 5500 Å och emissionsmaximum för FLV 100 på 6400 Å. Det finns

grönlysande dioder vars emissionsmaximum ligger vid 5500 Å (Hafo 1A48) men verkningsgraden hos denna är nära två tiopotenser lägre än FLV 100:s under det att känsligheten för CdS-motståndet vid 6400 Å endast har gått ned en faktor tre.

Med GaAsP lysdioden FLV 100 erhålles en bättre konstans av kalibreringen vid varierande ström genom dioden, se figur 11. Jämförande mätningar med glödlampan som ljuskälla och dioden som ljuskälla är gjorda på några material av rostfritt stål med olika ytavvikelse. För varje inställd ström till ljuskällan är systemet kalibrerat för fullt skalutslag vid mätning av referensytan. Av mätresultatet som redovisas i figur 12 framgår att endast ytor med mycket stor ytjämnhet ger utslag som faller inom felgränsen $\pm$ 10% (referens 2,3) då glödlampan användes som ljuskälla. Med dioden förbättras resultatet avsevärt och endast ytor med stor ytavvikelse ger utslag utanför felgränsen. Orsaken till de för låga utslagen är att antingen kommer resitansen i CdS-motstånden att falla utanför det linjära området eller blir resistansen så hög att förstärkarens inimpedans (Zin) ej längre är tillräckligt stor, se figur 13. Utbytes förstärkaren mot en vars ingångssteg har fälteffekttransistorer (Teledyne Philbrick 1421) kan mätområdet utökas.

Utbytet av glödlampa till lysdiod medför flera fördelar förutom en förbättrad korrelation mellan ytavvikelse och mätutslag. Effektutvecklingen är för glödlampan 2,4V·350mA= 840mW och för dioden 1,6V·40mA=64mW. Eftersom utrustningen skall vara ackumulatordriven medför detta en betydligt längre drifttid mellan uppladdningarna. Värmeutvecklingen i apparaten kommer också att minska avsevärt. Ytterligare

fördelar hos dioden är dess tålighet mot stötar, långa livslängd och dess mera punktformiga ljuskälla.

Jag vill framföra mitt varma tack till professor H.G. Grimmeiss som under arbetet har varit mig till stor hjälp med sin inspirerande handledning. Vidare vill jag tacka AB C.E. Johansson som ställt såväl glansmätare som provytor till förfogande.

Referenser:

1. IVF-Resultat 69609, Institutet för Verkstadsteknisk Forskning, 1969.

2. Mekan-Resultat 68505, Sveriges Mekanförbund 1968.

3. Bennet,H.E., IndustrialQality Control, No 8, 1964.

4. Motyčka, J., X Internat. Wiss. Koll. T H Ilmenau 1965.

5. Filiński, I, Physica Status Solidi (b), 49, 1972.

6. Schlötterer, H., Metalloberfläche, Heft 2,3 und 5, 1962.

7. Glansmätare 8510-1 C.E. Johansson, 1971.

8. Datablad för CL 705 HL-T, Clairex Electronics.

9. Moses A.J., Optical Materials Properties, Handbook of Electronic Materials, Vol 1, 1971.

Figurtexter.

1. Definition av ytavvikelse.
2. Definition av reflektionsvinkeln θ.
3. Goniofotometerkurva.
4. Polär-diagram visande det reflekterade ljusets intensitet som funktion av vinkeln.
5. Polär-diagram visande det reflekterade ljusets intensitet som funktion av vinkeln.
6. Det praktiska utförandet av det optiska systemet.
7. Intensitetensom funktion av fotonenergin för dels en glödlampa dels en lysdiod FLV 100, samt känsligheten som funktion av fotonenergin för ett CdS-motstånd. I diagrammet är också reflektionen gånger känsligheten inritad.
8. Mätuppställningen med Leiss-monokromatorn.
9. Reflektionen i förhållande till referensytan som funktion av fotonenergin.
10. Det reflekterade ljusets intensitet dividerat med det spridda ljusets intensitet som funktion av fotonenergin.
11. Kalibreringens förändring som funktion av strömmen genom ljuskällan.
12. Glansmätarens utslag som funktion av strömmen genom ljuskällan för olika provytor.
13. Kopplingsschema för kvotmätningen.

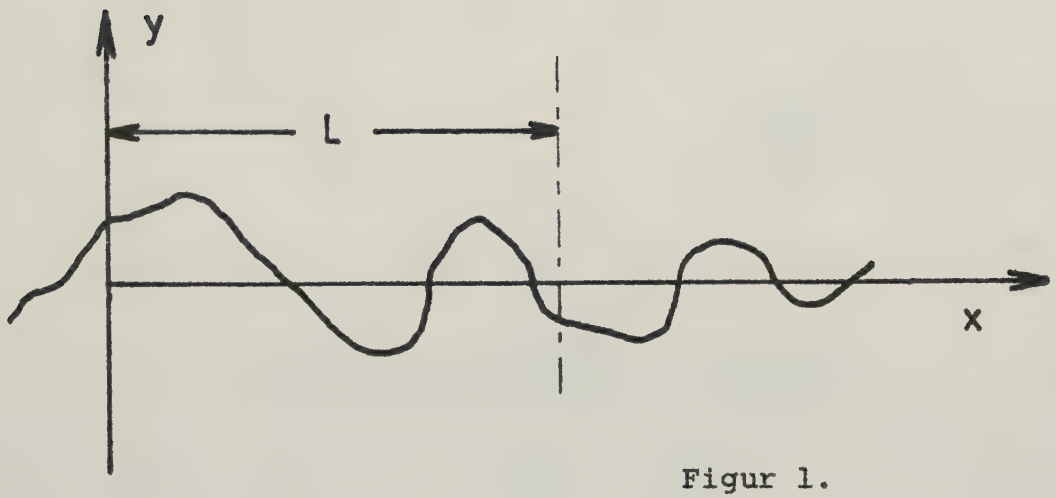

Figur 1.

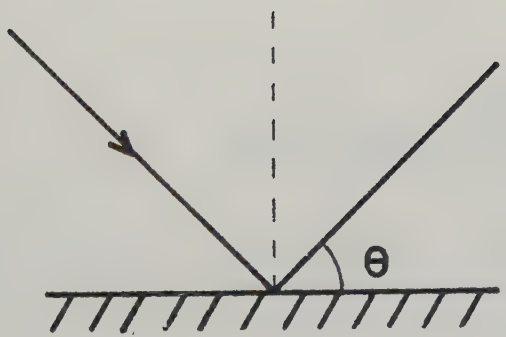

Figur 2.

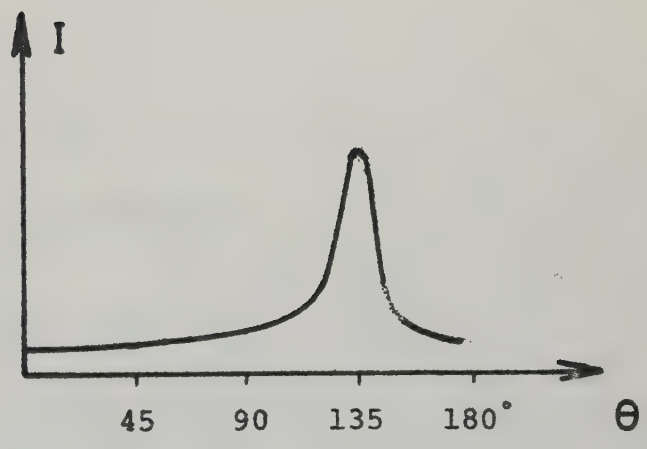

Figur 3.

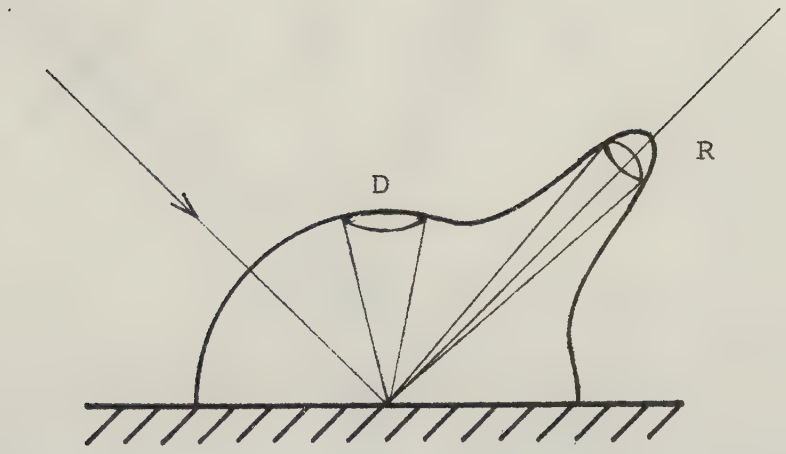

Figur 4.

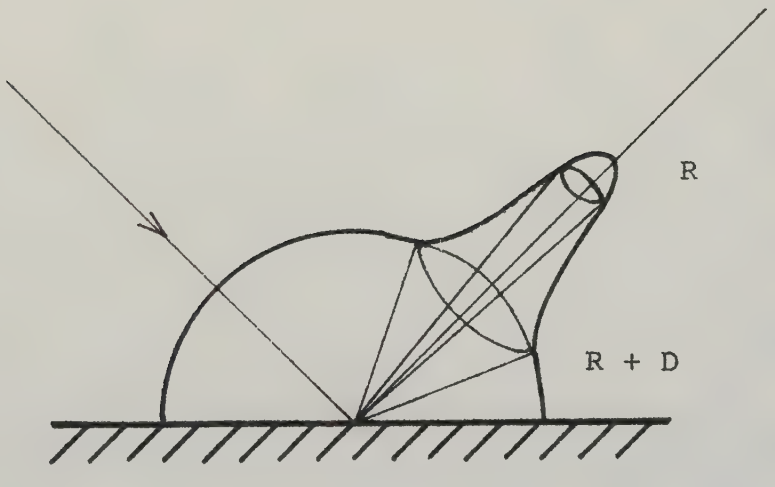

Figur 5.

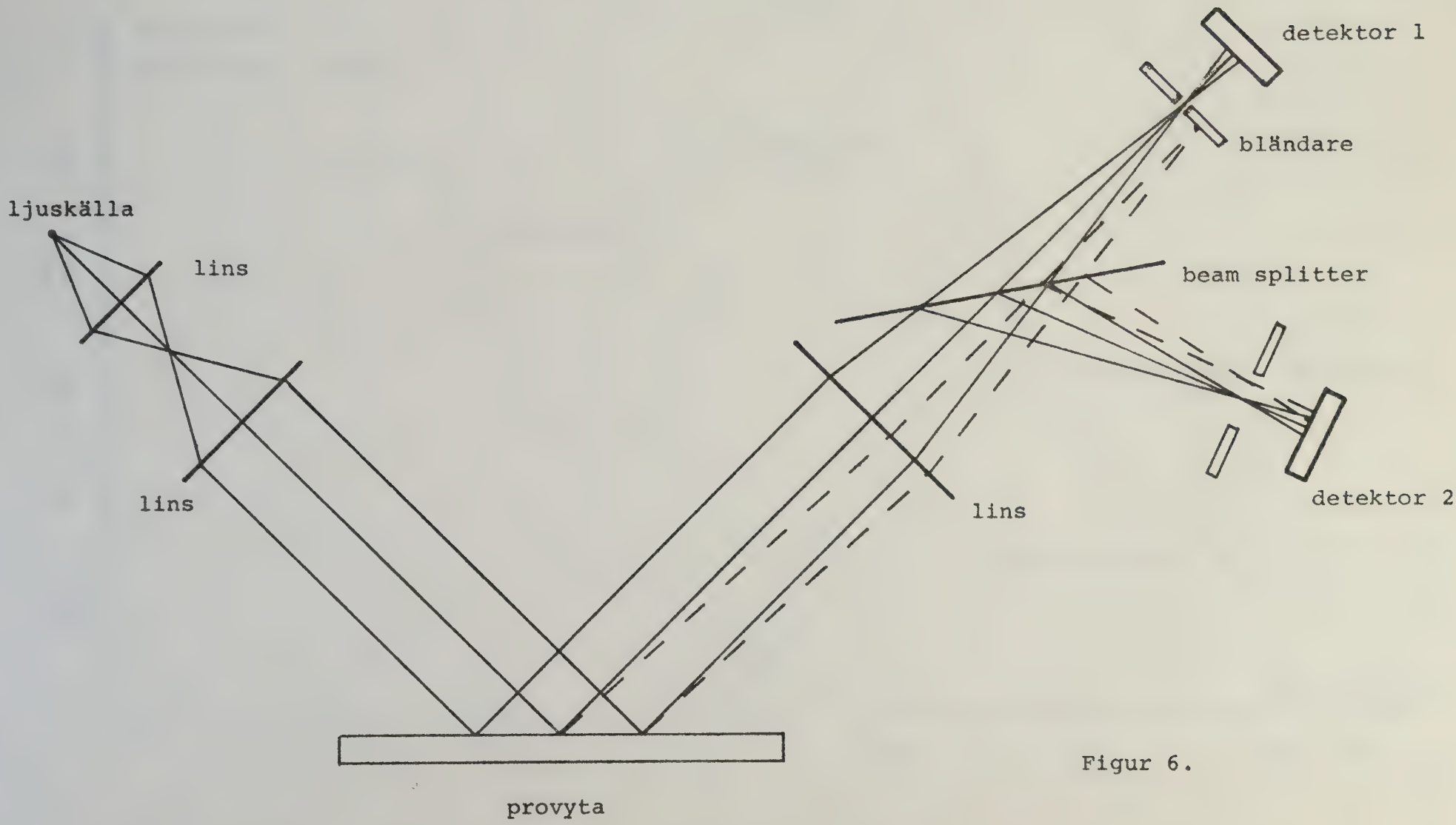
detektor 1
bländare
ljuskälla
lins
beam splitter
lins
lins
detektor 2
provyta

Figur 6.

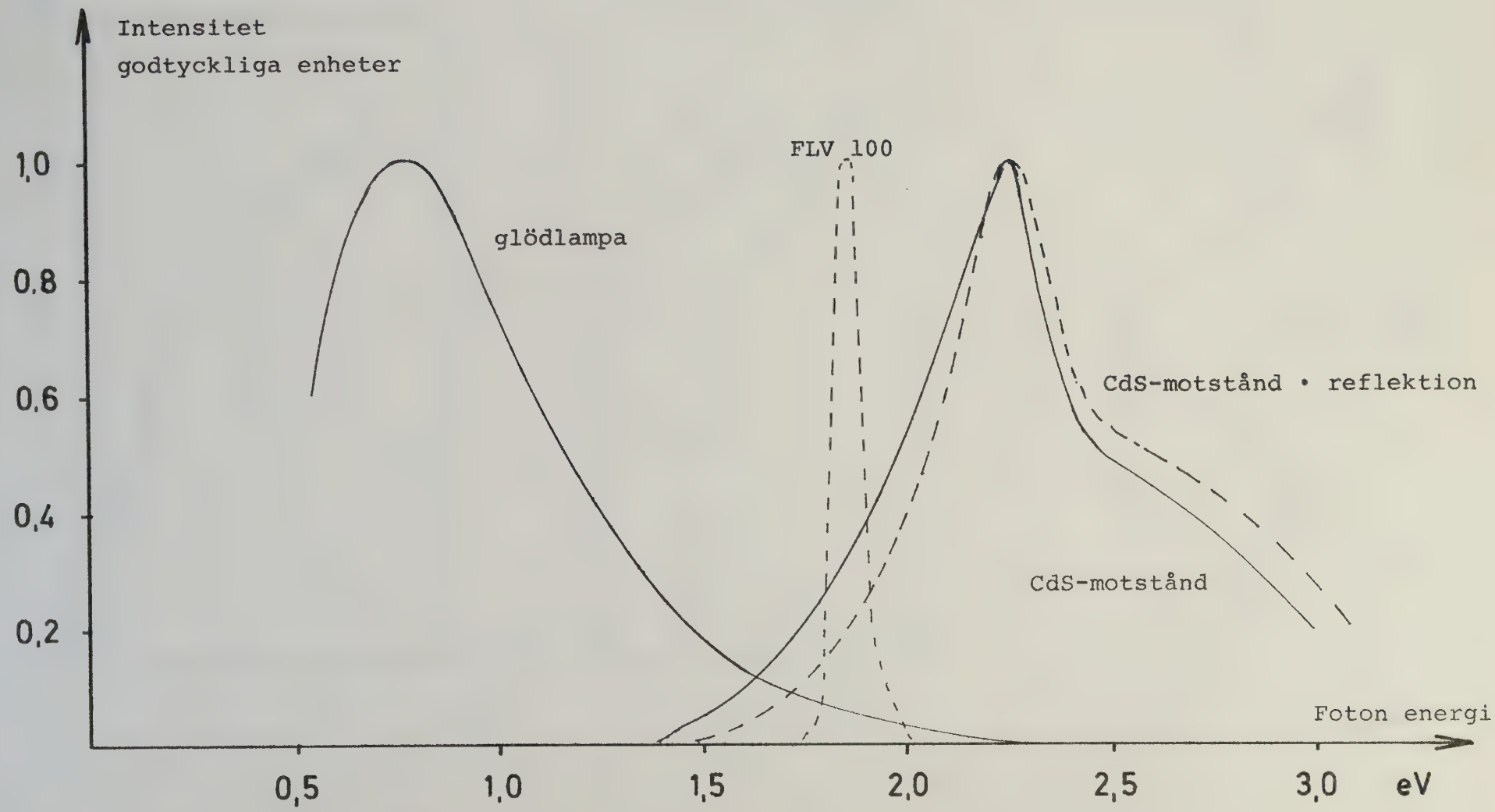
Intensitet
godtyckliga enheter
1,0
0,8
0,6
0,4
0,2
FLV 100
glödlampa
CdS-motstånd • reflektion
CdS-motstånd
Foton energi
0,5
1,0
1,5
2,0
2,5
3,0
eV

Figur 7.

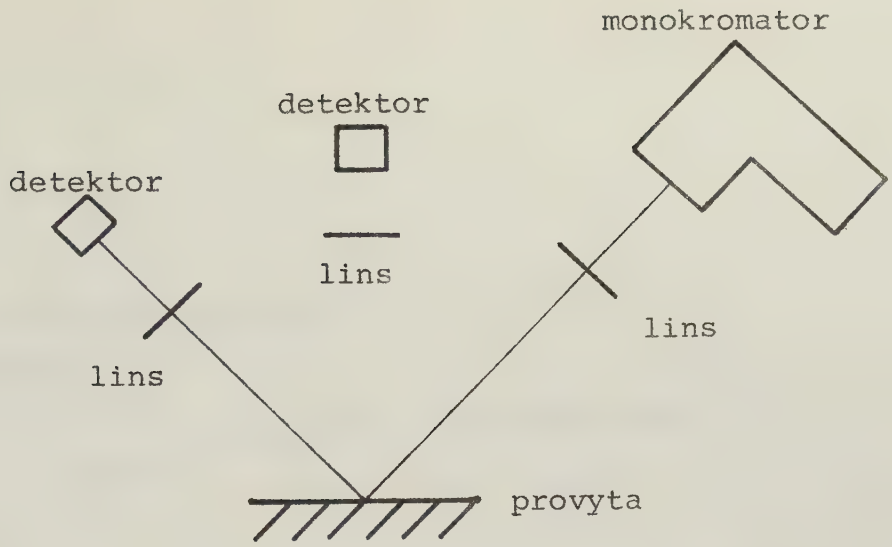

Figur 8.

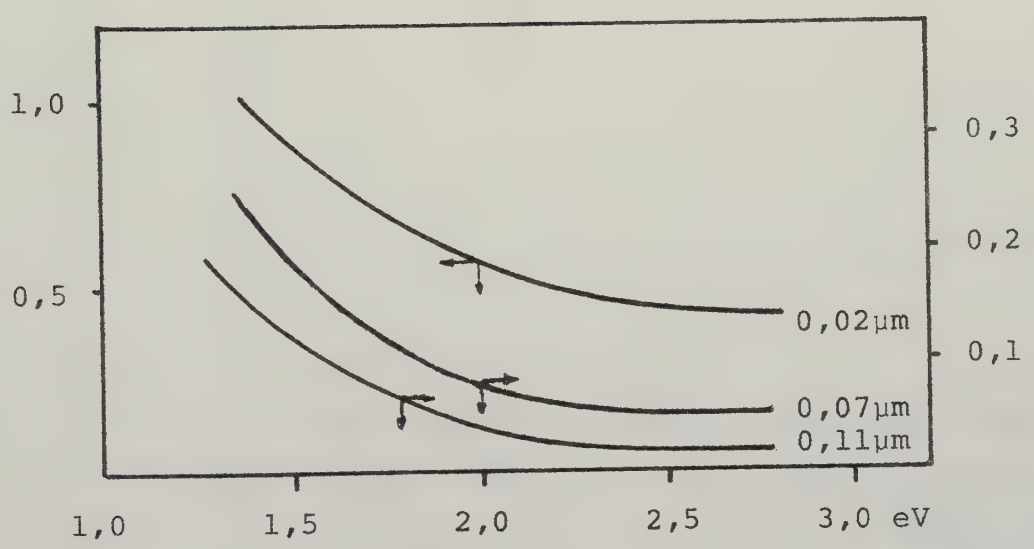

Figur 9.

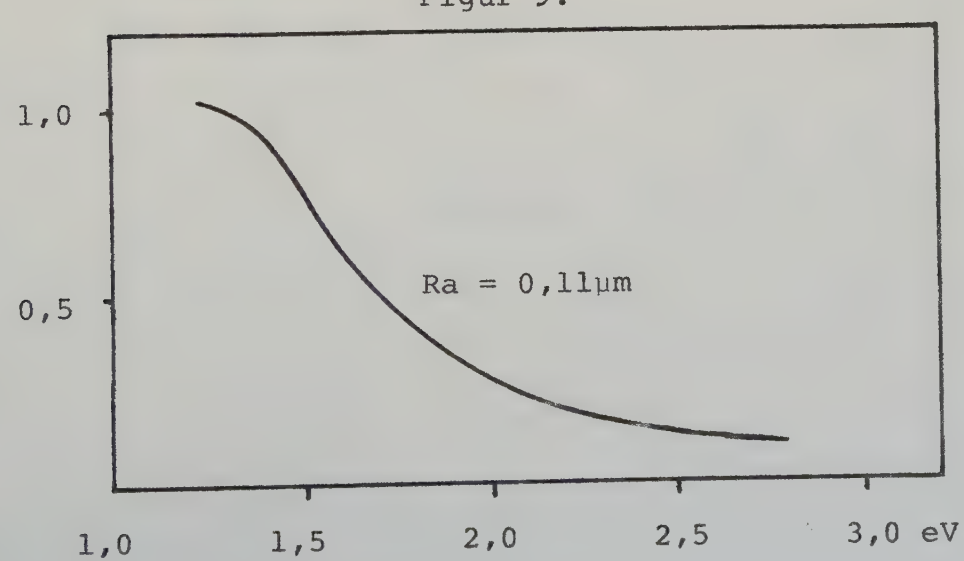

Figur 10.

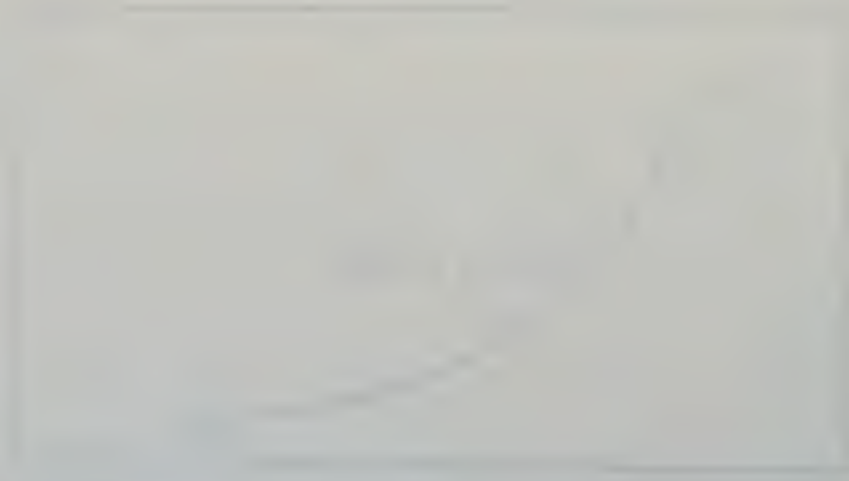

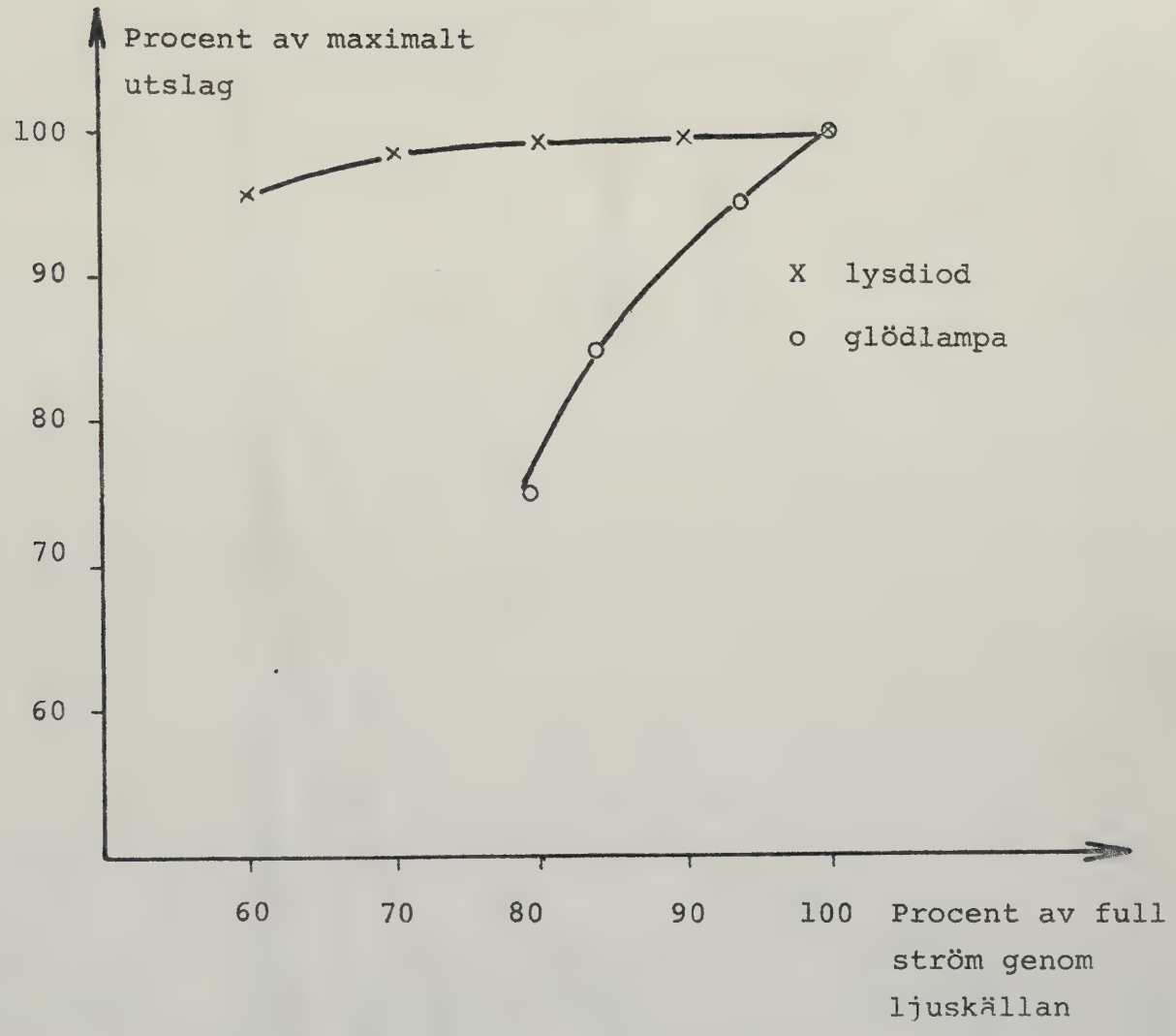
Procent av maximalt utslag
100
90
80
70
60
X lysdiod
o glödlampa
60
70
80
90
100
Procent av full ström genom ljuskällan

Figur 11.

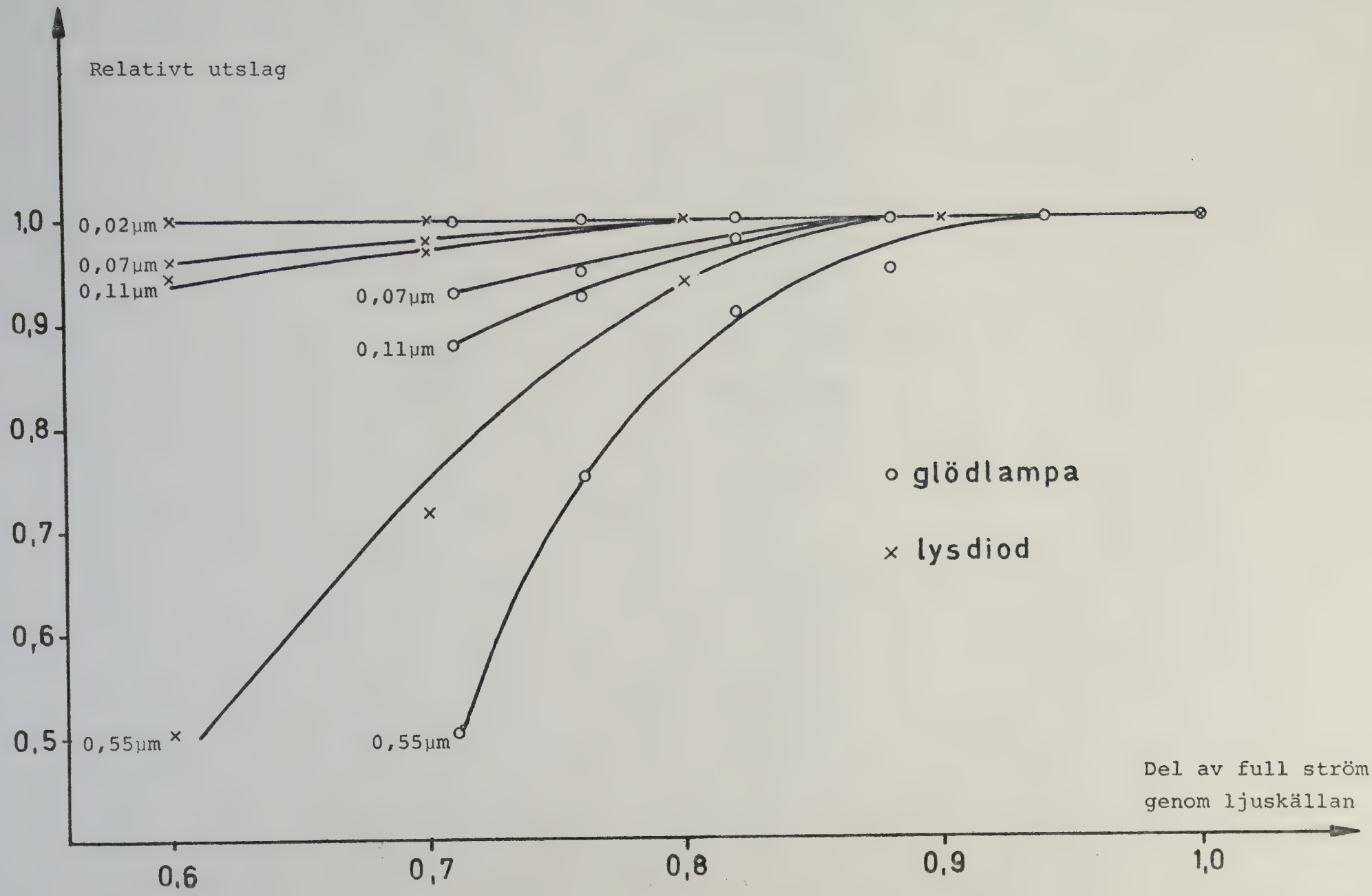
Relativt utslag
1,0
0,9
0,8
0,7
0,6
0,5
0,02µm
0,07µm
0,11µm
0,07µm
0,11µm
0,55µm
0,55µm
o glödlampa
× lysdiod
Del av full ström
genom ljuskällan
0,6
0,7
0,8
0,9
1,0

Figur 12.

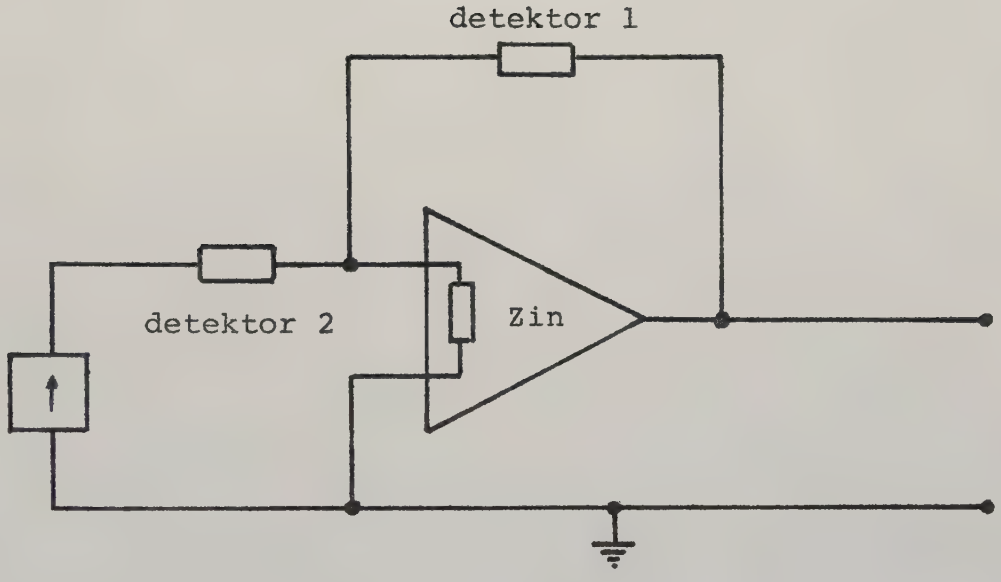

Figur 13.

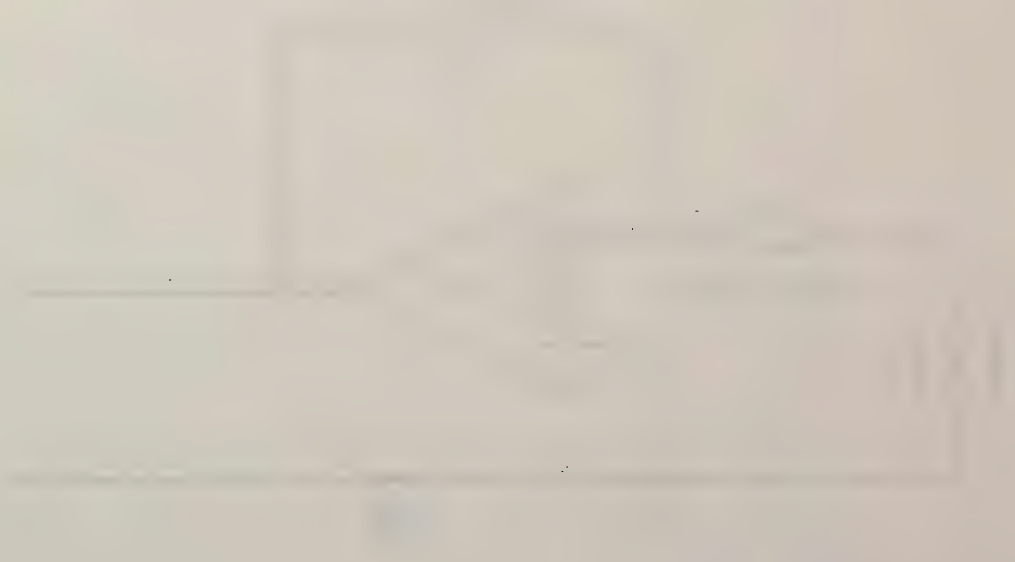

AN OPTO-ELECTRONIC SYSTEM FOR DETERMINING THICKNESSES AND DIAMETERS

Håkan Håkanson

Institute of Technology, Department of Solid State Physics, Fack 725, 220 07 LUND 7, Sweden

It is often desirable to measure the diameters or thicknesses of samples for which the measuring system must not be in mechanical contact with the speciment, e g the sample can be in motion or have a soft surface. The purpose of this paper is to present an opto-electronic system which satisfies these conditions. The limitations of some of the components in the system are also discussed.

The optical system is shown in figure 1. The rotating mirror is placed on the axis through the geometrical centre of the lenses and in the focal point of the first lens. This point has the property that any ray coming from it, or proceeding towards it, travels parallel to the axis after refraction. When the mirror is rotated the ray scans a particular area. The second lens brings the parallel incident rays to a focus, at which a detector is situated. The detector signal is amplified and fed to a logic system. If certain logic conditions are fulfilled, a pulse is generated at the output. This pulse starts and stops a counter which is driven in the time interval mode. When a sample is placed between the two lenses, the detector is not illuminated during the time it takes for the ray to sweep over the sample. This time is

measured and is proportional to the thickness of the sample. A silicon diode with an effective area of about two cm^2 is used as the detector. Its signal is amplified in an operational amplifier (Fairchild μA 741) and the complete circuit being shown in figure 2.

The output level of the circuit can be adjusted to zero for different light intensities of the room. This is done with potentiometer P1. The amplifier gain is determined by the resistors R4 and R3 and is approximately R3+R4/R3. Resistor R5 and Z1 protect the succeeding logic circuits against too high voltages and voltages of wrong polarity. The logic system must be able to distinguish between the two cases a) the detector is screened by a testsample or b) the rotating mirror is in such position that the rays do not pass through the first lens. This requirement can be solved in the following manner (figure 3). When the light falls upon the detector a reading pulse starts after a short delay. This remains at high level until a short time before the mirror removes the light from the detector. The logic condition which must be fulfilled for an output signal to be registered is that both the trigger signal and the reading pulse must be at high levels. The logic circuit which gives this condition is a NAND circuit. The delay of the reading-pulse and the fact that it is brought to a stop before the time measuring interval has fully elapsed is to eliminate any spurious signals generated during the switching period. Figure 4 is a schematic diagram showing the detector and the logic system. The Schmitt-trigger circuit is inserted to get small rise-and fall-times of the detector pulses. This

gives more accurate switching in the subsequent circuits.

With the rotating mirror driven by a synchron motor (Boone) and accuracy of better than $\pm$ 0.5% was achieved. The measuring range of the system is limited by the diameter of the lenses and is in our case 10-120 mm. In this range the linearity is better than $\pm$ 1%. The accuracy and linearity of the system, which can easily be improved, are limited by the stability of the motor, the precision of the lenses and the stability of the rise and fall-times of the detector. The rate of measurements is limited by the response time of the detector. If, for example, an octagonal mirror is used, the measuring rate is improved without increasing the speed of rotation. It is essential for the accuracy that all the planes of the mirror are in the focal point. To use a pin--diode which has a very fast response is not very convenient because of its small effective area. Most lenses with large diameters which are commercial available are plano-convex. To bring the spherical aberration to a minimum the lenses should be placed as in figure 5.

The chief feature of this system is that there is no mechanical contact with the sample which can also have a slow motion. This allows the system to be used for example in product control or, as in our case, to measure the extension of this tubes as a function of pressure. Through an external clock the counter display can be calibrated to present the result direct in millimetres. Furthermore the BCD output of the counter can be transformed to an analog signal which can be registered on a pen-recorder or an oscilloscope.

Acknowledgements

The author is greatly indebted to Professor H G Grimmeiss for valuable discussions concerning this work.

Figure Captions

Figure 1. The optical system

Figure 2. The complete circuit of the detector-amplifier

Figure 3. The pulses of the logic system as a functior of time. The amplitudes of the pulses are about 3 volts and the time scale about 300 μs per centimetre.

Figure 4. The schematical diagram of the logic system.

Figure 5. The ray tracing of the lens when the spherical aberration is at the minimum.

Component list to figure 2

Q1	Operational amplifier μA 741,	Fairchild
Z1	Zener diode 1N750A,	International Rectifier
P1	Potentiometer 10 turns,	Beckman Helipot
R1, R2	8.2 k	
R3	2.2 k	
R4	220 k	all resistors in ohms, 5%, 1/4 W
R5	68	

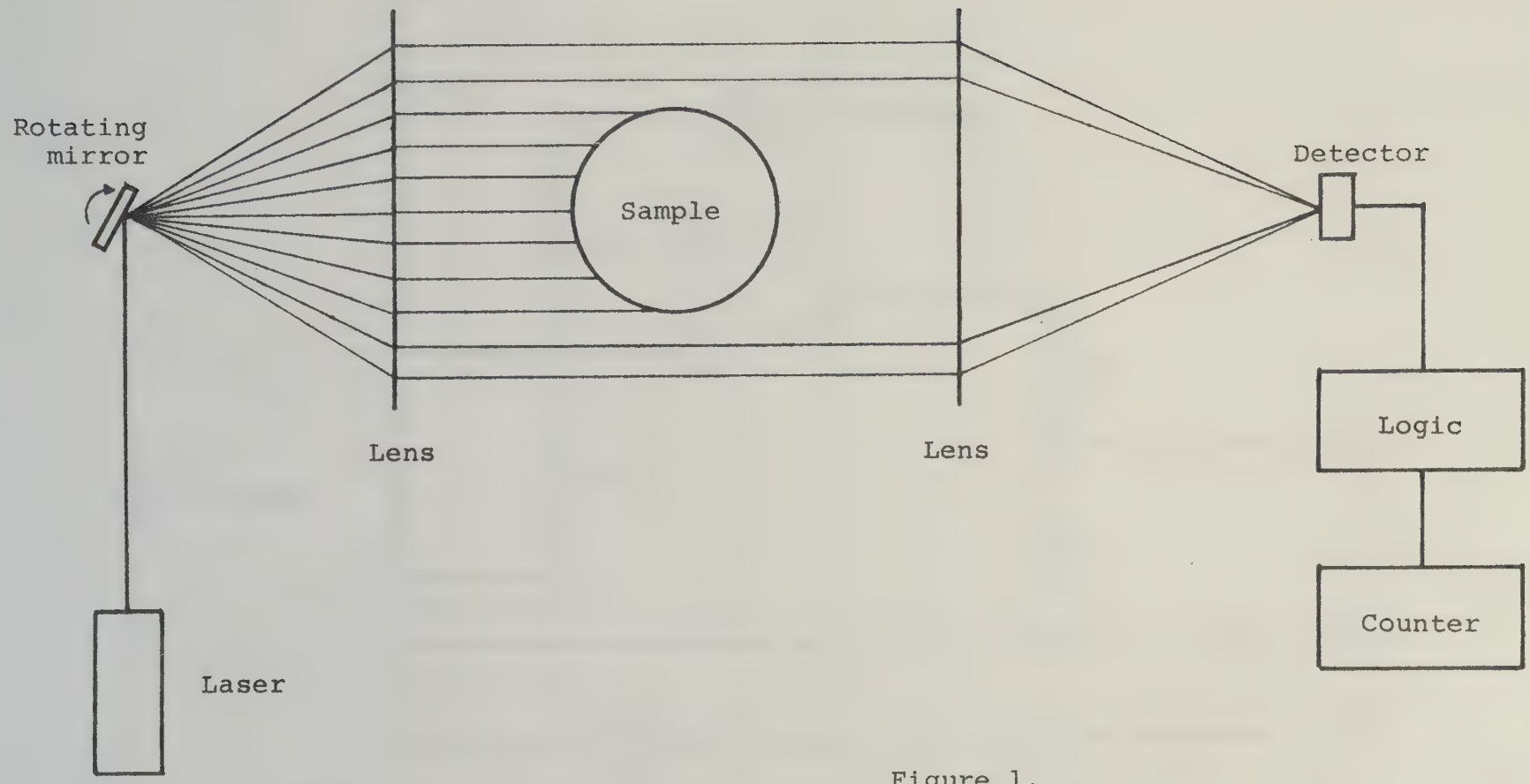
Rotating
mirror
Sample
Detector
Lens
Lens
Logic
Counter
Laser

Figure 1.

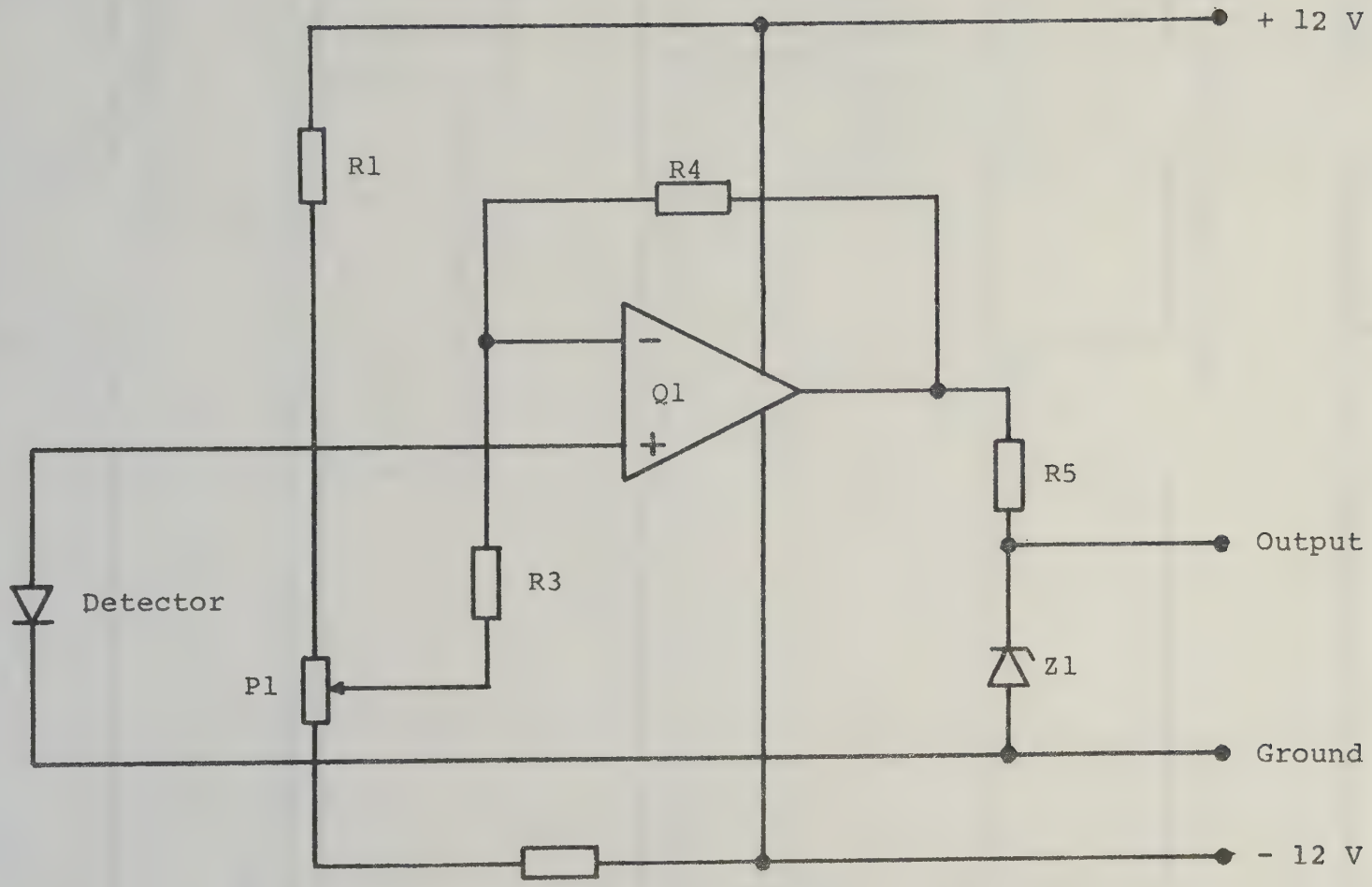

Figure 2

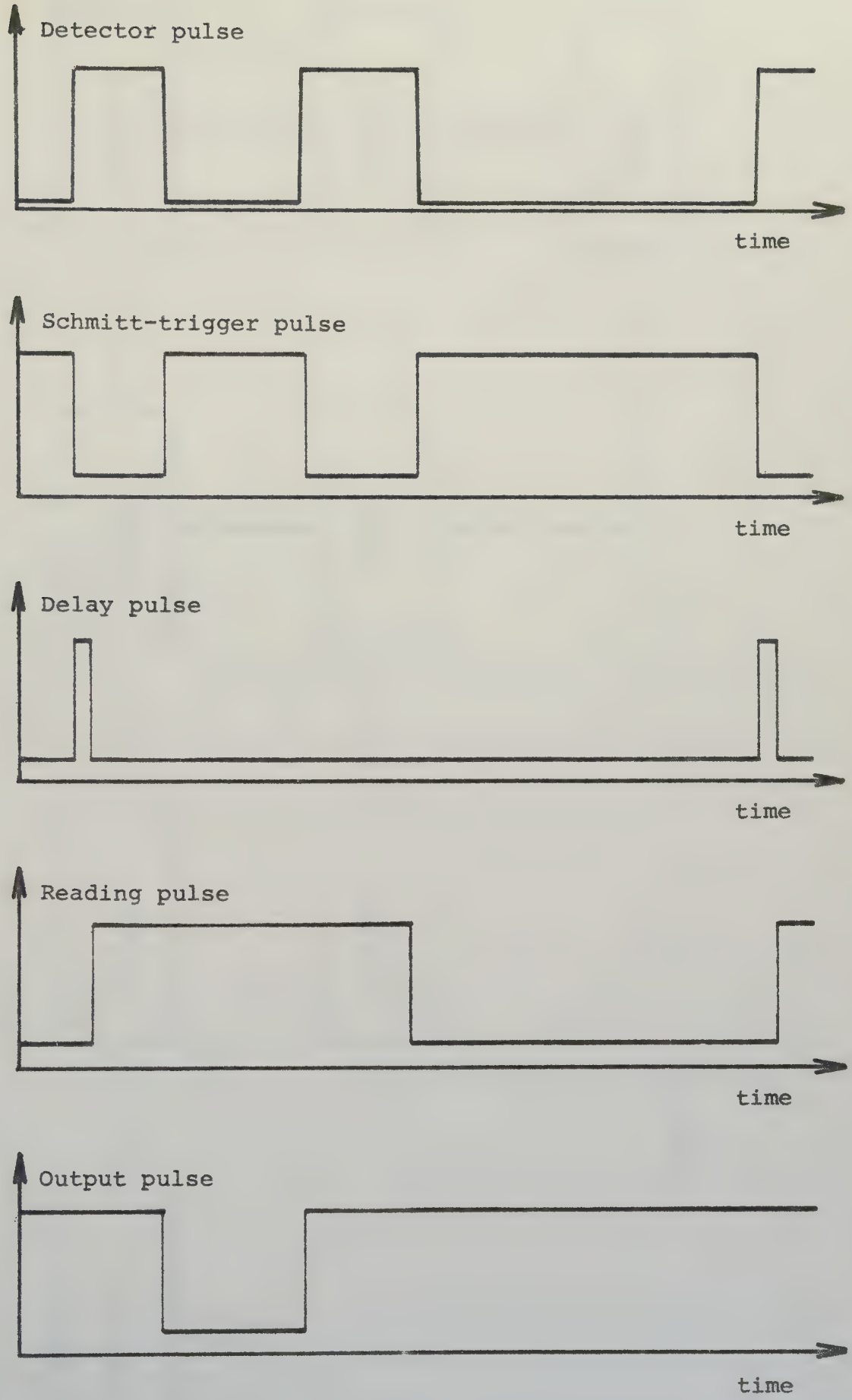
Detector pulse
time
Schmitt-trigger pulse
time
Delay pulse
time
Reading pulse
time
Output pulse
time

Figure 3.

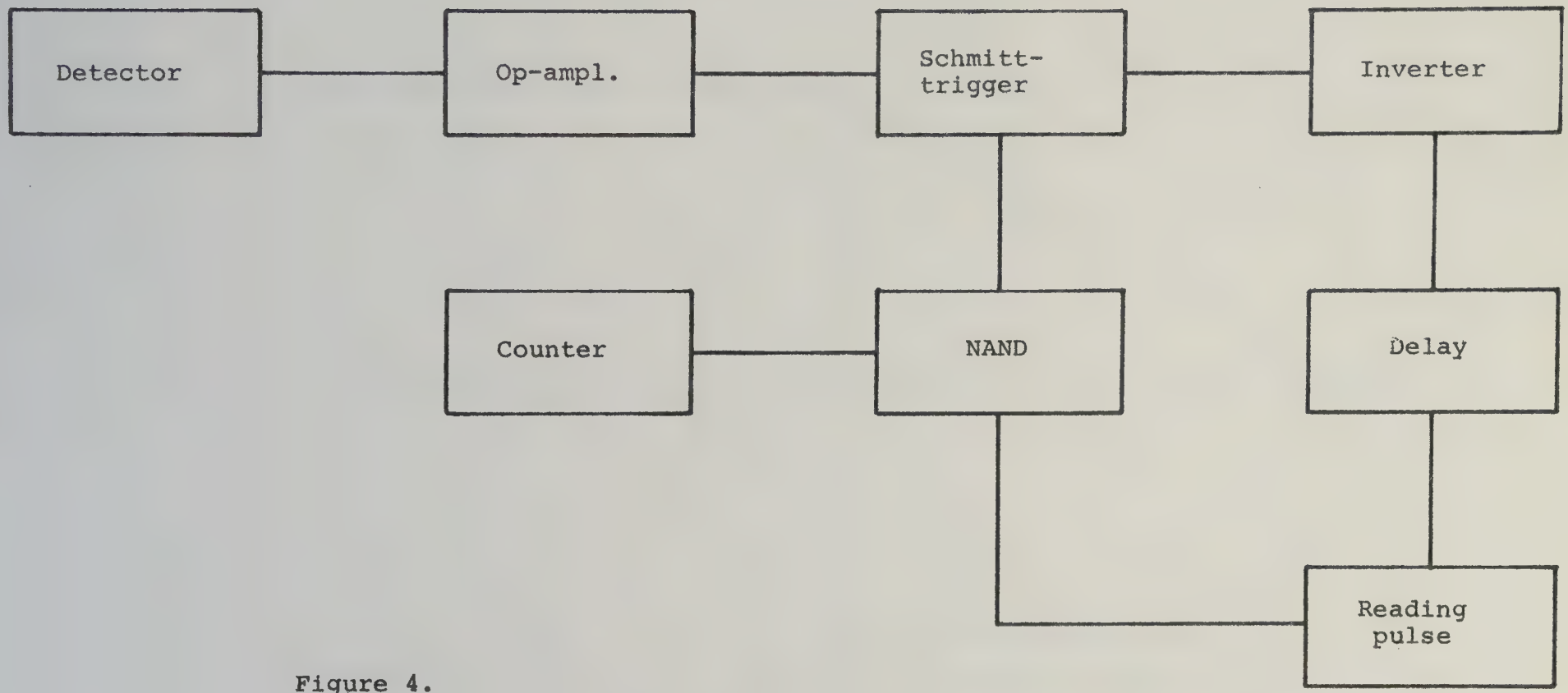
Detector
Op-ampl.
Schmitt-
trigger
Inverter
Counter
NAND
Delay
Reading
pulse

Figure 4.

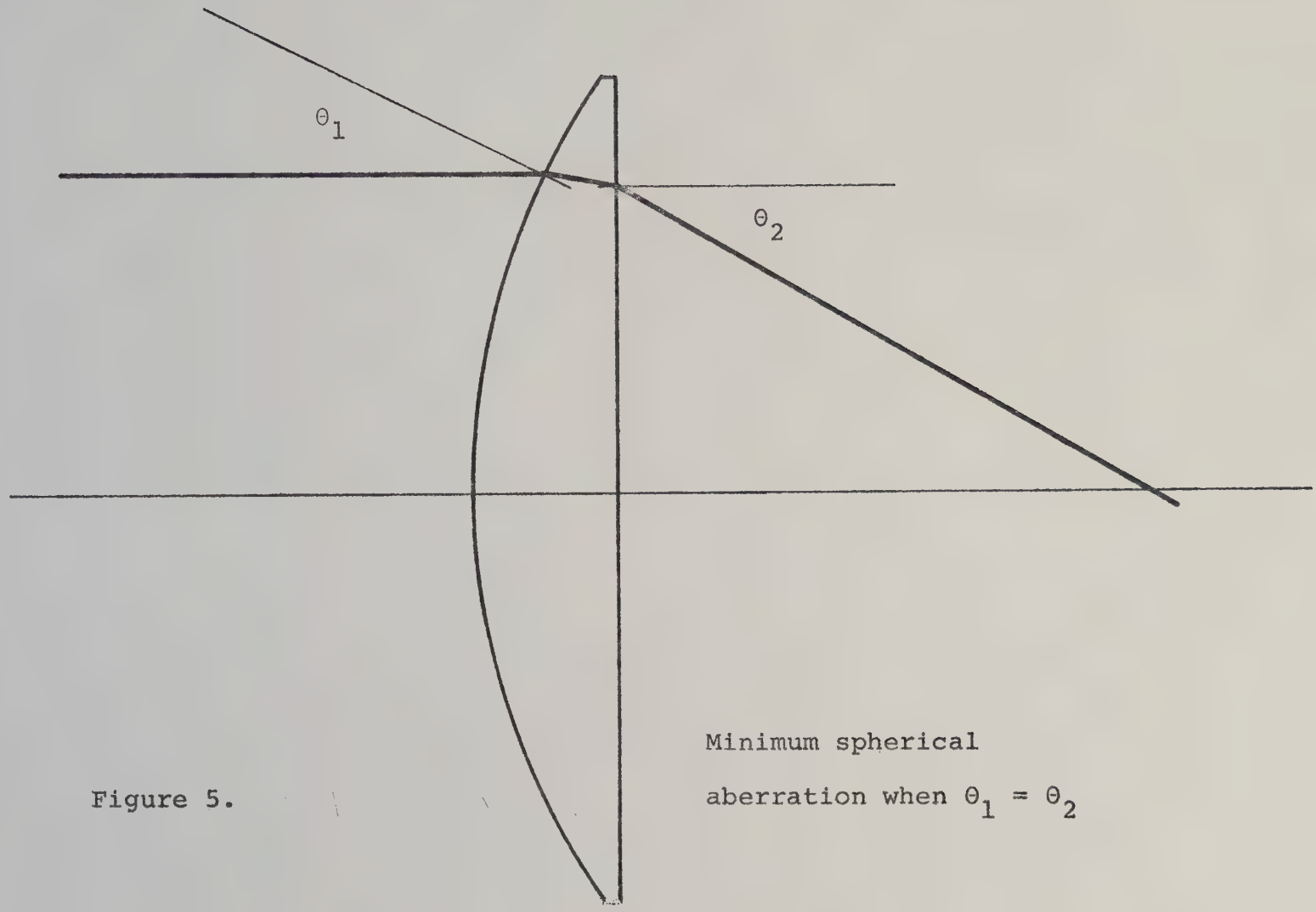

Figure 5. Minimum spherical aberration when $\Theta_1 = \Theta_2$

A photometer for measuring short tracks of heavy nuclei stopping in nuclear emulsion.

By

H. Håkansson, L. Jacobsson and G. Jönsson

Dept. of Physics, University of Lund, Lund, Sweden.

Abstract.

We discuss the technical and experimental details of a method which can be used both for a detailed study of the track width and for the determination of the charges of low energy, heavy particles. The track width is measured with a track photometer with a narrow slit and a revolving mirror system, which moves the image of the track across the slit. Different width parameters are discussed with regard to charge resolution.

1. Introduction.

In the domain of nuclear emulsion technique the charge of a particle must sometimes be determined when there is a residual range of the order of only 100 microns. Such ranges occur in solar cosmic ray measurements as multiply charged particles from the sun only exist in detectable amounts at low energies. (Fichtel and Guss 1961; Yagoda, Filz and Fukui 1961; Biswas, Fichtel and Guss 1962, 1966; Ney and Stein

1962; Pomerantz and Witten 1962; Biswas et al. 1963; Durgaprasad et al. 1968; Bertsch, Fichtel and Reams 1969; Beedle, Webber and van Allen 1971; Armstrong and Krimigis 1971; Bertsch et al. 1972). Bertsch et al. (1969) determined the abundance of the iron-group nuclei relative to oxygen in a solar cosmic-ray event using the δ-ray counting technique. This technique demands a projected minimum track length of 125 μm to get reasonable charge resolution. However, tracks of shorter ranges may add information to the discussion on solar particle acceleration and propagation mechanisms (Bertsch et al. 1972). It is accordingly important to work out methods of measurements which make possible charge identification at lower energies.

Another reason for studying stopping multiply charged particles is the possibility of getting information about the formation of the track of a charged particle passing through solid matter. Katz (1970) and Katz and Butts (1964) and Kobetich and Katz (1968,1969) have discussed the problems concerning track formation. A general track theory was developed which argues that the spatial deposition of energy by secondary electrons determines the track structure. Theoretical width-residual range relations were calculated in the range region 10 - 10^6 microns for a spectrum of charges. Measurements of individual tracks in G5-emulsions were compared with the teoretical width profiles. There seems to exist a fairly good agreement between the calculated and the experimental results. However, some uncertainty remains until the calculations are compared with measurements on tracks of particles which are identified with certainty.

In this report we discuss the experimental details of a method which can be used both for a detailed study of the

track width and for a determination of the charges of low energy, heavy particles. The method is studied by making measurements on tracks of well identified particles in a stack of Ilford G5 emulsions which was exposed to the primary cosmic radiation in a high altitude balloon flight. The track width has been measured with a nuclear track photometer, which will be described in the next sections. In the following sections there is a discussion of width parameters.

2. The photometric equipment.

The nuclear track photometer is of a type similar to the photometric instrument described by Kristiansson et al. (1967). This instrument was designed for carbon track measurements and it could not suitably be used for much wider tracks. Because it was important for us also to be able to measure tracks of Fe-nuclei, some improvements and modifications of the photometer were necessary.

2 A. The optical part.

The photometer construction is shown in fig. 1. The basic unit of the photometer is a Leitz Microscope, whose eye-piece has been replaced by an optical system with a narrow slit and a photomultiplier.

The objective and the lens L_1 form a real image of a segment of the track to be measured in plane A. Two pointers in plane A parallel to the x-direction of the microscope stage define the correct position of the track segment (Figure 2 a). The distance between the pointers is 1.3 mm corresponding to 13 microns in the emulsion plane if a 100x objective is used. The image of the track segment can be

adjusted relative to the pointers by micrometer screws moving the microscope stage in the x- and y-directions. The segment is adjusted parallel to the pointers by turning the upper part of the photometer around the bearing G. Because of this bearing small changes in the track direction, caused by Coulomb scattering, can be compensated for.

A semi-transparent mirror (beam splitter) placed above plane A divides the light beam into two parts. About 72% of the light is transmitted to the photomultiplier and about 28% is reflected to a reading microscope, Leitz MZ 25x, which is used for focusing the track segment in plane A.

The lens L_2 forms a new image in the plane B. In this plane there is a slit S parallel to the pointers with the dimensions 4.8 x 0.066 mm^2, which corresponds to 11.4 x 0.16 $micron^2$ in the emulsion plane (Figure 2 b). The slit is adjusted parallel to a straight line between the pointers in plane A. The light passing through the slit is spread over the cathode surface of the photomultiplier by a ground-glass plate lying closely above the slit. The diaphragms D_1 and D_2 are put into the tube to prevent reflections reaching the photomultiplier.

On its way between the lens L_2 and the slit S the light passes through a mirror system, which can be turned round a horizontal axis (Figure 3). The purpose of this system is to move the image of the track segment in plane B across the slit S. The mirror system consists of two front surface mirrors mounted on a common axis. The mirrors are parallel. Their inclination relative to the common axis is 37°. When the mirrors are turned, the beam of light is displaced and the image in plane B is moved. The speed of the image across the slit changes slightly with the angular position of the

mirror system. The dimensions of the mirror system are, however, so adapted, that the change of the speed of the image will be negligible for a rotation within ± 20° of the zero position. This rotation gives rise to a movement of the track image in plane B, which corresponds to a distance of about 80 microns in the emulsion plane if a 100x objective is used.

The mirror system is turned by a Berger synchronous-motor RSM 48, which can rotate both in the forward and in the reverse direction. The rotational speed of its driving axle is 60 r.p.h.. The rotation is transmitted to the mirror system and reduced to 15 r.p.h. by friction-connected gear-wheels.

The amount of light passing through the slit depends upon the light absorption in the area of the emulsion covered by the slit. As the image of the track segment is moved across the slit the amount of light reaching the photomultiplier will fluctuate. The light intensity is recorded with a pen-recorder, which gives an absorption profile of the track segment. Some examples of such profiles are given in Figure 4a.

2 B. The electronic system.

The electronic system converts the intensity of the light through the upper slit into an amplified d.c. voltage, which in turn is registered by a pen-recorder. Moreover there is a reference current source for test of linearity.

The photomultiplier. We have chosen an EMI 9524 B photomultiplier as the detector. The resistance values of the dynode chain are determined by the two conditions: the chain

current chosen must be sufficiently high to get linearity; the heat dissipated because of the chain current must not heat the tube and cause a change in the current. These conditions are fulfilled if the chain current is 2 mA. The voltage stability of the first dynode, which is the most critical one, is ensured by using a Zenerdiode.

A 1% change in the supply voltage will cause a 8% change in the anode current. Therefore we have chosen a stabilized high voltage power supply (Oltronix LS 529 R). This has a stability of $3 \cdot 10^{-5}$ for a 10% change in the line voltage.

The d.c. amplifier. The signal from the photomultiplier is fed through a direct current (d.c.) amplifier. It is important for the amplifier to have low input impedance so as not to affect the input signal. As the output of the amplifier is connected to a pen recorder the input impedance of the recorder and its short response time make demands upon the amplifier.

Low input impedance is achieved in the circuit in Figure 5 by the feedback resistor R_f. As a first approximation the input impedance Z_{in} of this circuit is $Z_{in} = R_f/A$ where R_f is the feedback resistor and A is the open loop gain of the amplifier (De Waard and Lazarus 1966). The output voltage V_{out} of the amplifier is given as the input current (i_{in}) times the feedback resistor (R_f).

To decrease the sensitivity of the amplifier to input transients the feedback resistor must be shunted with a smoothing capacitor (C_f). This will increase the response time of the amplifier. However, we have chosen the capacitance, C_f, so that the RC time is short compared with that of the recorder.

The photomultiplier gives currents of the order of 0.1 to 100 μA. As we want the error from the amplifier to be below 0.1%, the input bias current must not exceed 10^{-10} A.

The maximum variation of the temperature, Δt, in the room where the amplifier is used, is ± 2.5°C. To keep the required accuracy, the product of the temperature coefficient of the amplifier and Δt must be less than 100 pA.

The complete circuit is shown in Figure 6. We have chosen the Philbrick Operational Amplifier 1009, which has a maximum input bias current of 30 pA and a maximum input bias current drift with temperature of 3 pA/°C. Both values are within the allowed range for the required accuracy. As the dependence of the bias current on the supply voltage is as low as 5 pA/V there is no need for a high stability power supply.

To protect the amplifier against too high voltages, we shunted the input with two low leakage diodes, one in each direction.

The output resistance of the amplifier is low enough to feed the recorder, which has an input impedance of at least 0.5 megohm.

Reference current source. It is desirable to be able to test the linearity of the amplifier and recorder. Therefore the system also includes a variable current source. The general principle is shown in Figure 7.

The lead current passes through the sensing resistor R_s and the voltage across R_s is compared with the reference voltage. The difference between these voltages is amplified and fed to the series regulator, which adjusts the current to the set value.

The current source must have a high resistance so that variations in the load resistance R_L do not affect the current. For our circuit the source resistance can be calculated in the following way. A change in load current, Δi_L, makes a change $\Delta i_L \cdot R_s$ in the voltage drop across R_s. If the amplifier gain is A we receive a change Δv in the output signal from the amplifier which is $\Delta i_L \cdot R_s \cdot A$. As the voltage gain in the series regulator is close to unity, the output voltage from the series regulator is also approximatly equal to $\Delta i_L \cdot R_s \cdot A$. This gives the source resistance $R_{out} = A \cdot R_s$.

The complete circuit is shown in Figure 8. To cover the range of the amplifier the source must be able to supply currents between 10^{-7} and 10^{-4} A. The maximum temperature range (Δt) is as before $5^{o}C$. The temperature drift of the amplifier has a maximum of 75 $\mu V/^{o}C$, which gives a maximum drift of 0.4 mV for the whole temperature range. As the voltage drop over the sensing resistor R_s is 1.2 V for full current output, the error is less than $4 \cdot 10^{-4}$.

The current is adjusted with a ten-turns precision potentiometer, which has a linearity better than $2.5 \cdot 10^{-3}$.

The reference voltage in the current source is provided by the reference diode IN823 IR. This diode has a temperature stability of $5 \cdot 10^{-5}/^{o}C$, which is sufficiently low for our purpose. In order not to be disturbed by changes in the line voltage, the current source has a highly stabilized power supply DA 120. The voltage change is ± 0.5 mV for a ± 10% change in the line voltage.

The pen recorder. An Esterline Angus 10 inch single channel potentiometer recorder (E 1101 S) is used as the recording instrument.

It is important for our application to have a recorder with short time for full scale deflection and good accuracy. The specification for our recorder is 0.2 sec for full scale deflection and an accuracy of ± 0.4% of full scale for any range.

2 C. Tests of the photometer.

It is desirable that the image of the track segment moves with constant speed across the slit S. We checked this by measuring several consecutive lines of an object micrometer, which replaced the emulsion. The distance between the absorption profiles is a measure of the speed of the image across the slit. The change of the speed was found to be less than 0.5% for rotations of the mirror system within ± 15^{o}. This angle corresponds to a displacement of about 50 microns in the emulsion plane if a 100x objective is used.

We have also tested how well a track was focused in plane B when focused in plane A, by studying profiles of the same track segment in measurements with different degrees of defocusing. The area Y and the height h of the individual profiles were measured and Y/h was calculated. This quotient is expected to reach its minimum value when the image is well focused on plane B. It was found to be at a minimum when the track segment was focused in plane A. Consequently the image in plane A and the image in plane B were focused simultaneously.

We checked that the slit S and the line defined by the two pointers were parallel. Profile measurements were made on micrometer lines, with different angular positions of the upper part of the photometer. The quotient, Y/h, of these

profiles was found to have its minimum value when the lines of the micrometer were parallel to the pointers. This minimum indicates that the slit lies parallel to the pointers.

For three different paper speeds, 2, 1 and 1/2 inch/s, profile measurements were made on a line of an object micrometer. The result of ten measurements of the quotient Y/h at each speed is shown in Table 1. We conclude that Y/h is changed

Table 1

SPEED (Inch/s)	2	1	1/2
Y/h	4.68 ± 0.01	2.33 ± 0.02	1.18 ± 0.01

by the same factor as the speed of the recorder within the statistical errors. It is thus possible to use different speeds when measuring different tracks. In the measurements described below the paper speed is kept at the constant value 1 inch/s.

3. Possible track width parameters.

The track width can be described by different parameters. Which parameter is most suitable in a certain case depends on the purpose of the measurement. In charge determinations the paremeter Y/h (called mean track width, MTW) is found to give satisfactory charge resolution (Kristiansson et al. 1967). By suitable calibration this parameter can be expressed in microns. However, such a transformation is somewhat questionable as it is difficult to understand what MTW really means. In measurements of track width not far from the end of the

tracks we have also found it suitable to use the profile width at one half, at one third and at two thirds of the height of the profile, $W_{1/2}$, $W_{1/3}$ and $W_{2/3}$, as track parameters (Figure 4 b).

3 A. Width measurements on lines.

To study the response of the instrument we have made profile measurements on narrow lines on a glass plate. The four parameters MTW, $W_{1/2}$, $W_{1/3}$ and $W_{2/3}$ were determined for each profile. The number of measurements on each line width was large enough to get negligible statistical errors. The values of the width parameters obtained are compared with the width of the lines in Figure 9. The relations are linear. Their graphs do not coincide and do not pass through the origin. The reasons are the non-negligible response time of the recorder and the finite width of the slit.

The diagram in Figure 9 shows what the widths of lines will be, when translated by the photometer into the four above-mentioned parameters. By means of this diagram it is possible to relate the parameter which describes the width of a track segment to a metric scale.

3 B. Width measurements on tracks.

Measurements were made on tracks of stopping carbon, magnesium and iron nuclei. Five tracks were picked out from each group. The dip angles, α, of these tracks in the undeveloped emulsion were below 10° ($\tan \alpha \leq 0.17$). The distance from the track to any edge of the pellicle was larger than 10 mm so as not to get distorted measurements because of edge effects. Furthermore the parts of the tracks measured were not closer than 35 microns to the glass or the sur-

face of the emulsion. The charges of the nuclei had been identified in other investigations (Dellien 1969, Jönsson et al. 1970).

A profile was registered every 10 microns for each track in the range-regions 5-105, 175-225, 275-325 and 375-425 microns. In order to calculate the parameters MTW, $W_{1/3}$, $W_{1/2}$ and $W_{2/3}$ from the individual profiles, base lines were drawn for every profile. These base lines are intended to represent the light background in the pellicle if no track was present. The base lines, dotted in Figure 4a, are always drawn as straight lines connecting the estimated background lines on both sides of the profile. Although a straight base line is not always suitable to represent the background level in all types of profiles, it is usually a good approximation (Kristiansson et al. 1967).

In Figure 10 the mean value of each parameter is plotted as a function of residual range. In Figure 11 the mean values are transformed into widths in microns by means of the graphs in Figure 9. Objections on this transformation can be made. A track segment has irregular edges and δ-rays are jutting out. The transformation implies, however, that the segment is directly compared with a corresponding line segment being compact and having smooth edges. Furthermore the lines are two-dimensional while a track is three-dimensional, which means that additional systematic errors may be introduced.

4. Discussion.

Comparisons between the width parameters. The four different parameters are plotted as a function of the residual range in Figure 10. We notice that for the same charge, the curves

representing the different parameters differ from each other. This indicates a possibility of different capacity for particle identification and also a possibility for a discussion of the track structure. In Table 2 we have calculated the quotients

$$\frac{W_x(R_v,Z_i)}{W_x(R_v,Z_j)}$$

where W_x is $W_{1/3}$, $W_{1/2}$, $W_{2/3}$ or MTW. R_v is the residual range and $Z_{i,j}$ is the charge.

The standard errors of the quotients depend somewhat on range and charge. The relative standard error is less than 10%.

Table 2 shows that the individual quotients do not differ from each other for the different parameters when compared at the same residual range (R_v) and for the same pair of charges (Z_i/Z_j). Consequently the measured parameters give approximately the same amount of useful information for particle identification in the range which we have studied

Table 2. Quotients between track parameters.

Z_i/Z_j	Z=12/Z=6				Z=26/Z=6				Z=26/Z=12			
R_v(μm)	MTW	$W_{1/3}$	$W_{1/2}$	$W_{2/3}$	MTW	$W_{1/3}$	$W_{1/2}$	$W_{2/3}$	MTW	$W_{1/3}$	$W_{1/2}$	$W_{2/3}$
50	1.4	1.4	1.3	1.5	2.1	2.0	2.0	2.1	1.5	1.4	1.5	1.5
100	1.6	1.6	1.6	1.7	2.8	2.7	2.7	2.9	1.7	1.7	1.7	1.8
150	1.7	1.8	1.7	1.8	3.3	3.4	3.3	3.7	1.9	1.9	1.9	2.0
200	1.8	1.9	1.8	1.9	3.8	3.8	3.9	4.2	2.0	2.1	2.1	2.2
300	2.0	2.1	2.0	2.0	4.3	4.6	4.6	4.8	2.2	2.2	2.3	2.4
400	2.0	2.2	1.9	1.9	4.8	5.0	4.5	4.7	2.3	2.3	2.4	2.4

Charge resolution. In the study of low energy solar particles it is of great importance to be able to separate tracks

of nuclei with different charges at residual ranges below 100 μm. We have determined the charge resolution at different residual ranges for the four parameters. For each track the sums of the parameter values within the range interval $R_o \leq R \leq R_1$ have been calculated. If the mean value of these sums for a charge Z_i is $S_i(R_1)$ and its standard error is $\sigma_i(R_1)$ the charge resolution $\Delta Z_i(R_1)$ is with good accuracy found to be given by

$$\Delta Z_i(R_1) = \frac{(Z_i - Z_j) \cdot \sigma_i(R_1)}{S_i(R_1) - S_j(R_1)} \qquad (i \neq j).$$

In Figure 12 $\Delta Z_i(R_1)$ is shown as a function of R_1 for the measured charges Z = 6, 12 and 26. R_o is put equal to

$$\begin{cases} 10 \text{ μm for } R_1 \leq 100 \text{ μm} \\ 100 \text{ μm for } R_1 > 100 \text{ μm} \end{cases}$$

In the Figure 12 the curves for $W_{1/2}$ are given. The curves for the other parameters are similar to that of $W_{1/2}$, which can be expected from Table 2.

From Figure 12 we conclude that ΔZ is less than about 2 units of charge at 50 microns residual range. It may therefore be possible to separate tracks of the iron group nuclei from those of the rest of the spectrum at this order of residual range in emulsions exposed to solar cosmic rays.

Comparison with the measurements with a filar micrometer.

One of us (G.J.) measured all the tracks studied in our investigation again using a filar micrometer. The total magnification was 1200 X. For the measurement of each segment of a track the filament was adjusted with regard to the δ-rays of the segment. The convention applied was, in short: the space between the track and the filament not filled by grains belonging to the track must have a projected area equal to

that of the grains outside the filament and also belonging to the track. Every track segment was measured four times to reduce the personal errors. The projected length of a segment, along which the filament was adjusted, was 12 μm for residual ranges $R \leq 100$ μm and 90 μm for $R \geq 100$ μm.

The width values from the filar micrometer measurements are also plotted in Figure 11. In a comparison between the filar micrometer measurements and the photometer measurements one sees small differences which seem to be systematic. Part of the explanation of that may be the subjective convention. One important difference between the two types of measurements is that the micrometer measurements are two-dimensional whereas the photometer measurements are light absorption measurements, which also register defocused grains.

The authors wish to thank Dr K Kristiansson for valuable help.

References.

T P Armstrong, and S M Krimigis, 1971;
Johns Hopkins Applied Physics Laboratory preprint.

R E Beedle, W R Webber, and J A Van Allen, 1971;
Trans. Am. Geophys. Union, 52, paper SC3, p.311.

D L Bertsch, C E Fichtel, and D V Reames, 1969;
Ap.J. (Letters), 157, L53.

D L Bertsch, C E Fichtel, and D V Reames, 1972;
Ap.J. 171, 169.

S Biswas, C E Fichtel, and D E Guss, 1962;
Phys. Rev. 128, 2756.

S Biswas, C E Fichtel, and D E Guss, 1966;
J. Geophys. Res. 71, 4071.

S Biswas, C E Fichtel, D E Guss, and C J Waddington, 1963;
J.Geophys. Res. 68, 3109.

U Dellien, K Söderström, and K Kristiansson, 1970;
Astrophys. Space Sci. 8, 74.

H DeWaard, and D Lazarus, 1966;
Modern electronics p.192. Addison Wesley.

N Durgaprasad, C E Fichtel, De Guss and D V Reames, 1968;
Ap.J., 154, 307.

C E Fichtel, and D E Guss, 1961;
Phys.Rev. Letters, 6, 495.

G Jönsson, K Kristiansson, and L Malmqvist, 1970;
Astrophys. Space Sci. 7, 231.

R Katz, 1970;
Paper presented at 7th international colloquium on corpuscular photography and visual solid detectors, Barcelona, 1970.

R Katz, and J J Butts, 1964;
Vth international conference on nuclear photography Cern.

R Katz, and E J Kobetich, 1969;
Phys. Rev. 186, 344.

E J Kobetich, and R Katz, 1968;
Phys. Rev. 170, 391.

E J Kobetich, and R Katz, 1968;
Phys. Rev. 170, 405.

K Kristiansson, A Ladd, and L Malmqvist, 1967;
Arkiv Fysik 34, 139.

E P Ney, and W Stein, 1962;
J.Geophys Res. 67, 2087.

M A Pomerantz, and L Witten, 1962;
paper presented at the 3rd Int. Space Sci. Symp. of COSPAR, Washington, D.C.

H Yagoda, R Filz, and K Fukui, 1961;
Phys. Rev. Letters, 6, 626.

Figure captions.

Fig. 1. The main features of the optical part of the photometer. The diagram to the right shows the upper part of the instrument from the front. The left-hand drawing shows a sideview.

Fig. 2a. Slit plane A seen through the reading microscope Leitz MZ. The position of the image of the track section to be measured is defined by the two pointers.

b. Slit plane B with the image of a track section.

Fig. 3. The mirror system.

Fig. 4a. Examples of track profiles of an iron nuclei at different residual ranges.

b. An illustration of the parameter values $W_{1/3}$, $W_{1/2}$ and $W_{2/3}$.

Fig. 5. Principal circuit of the amplifier.

Fig. 6. Complete circuit of the amplifier.

Fig. 7. Principal circuit of the current source.

Fig. 8. Complete circuit of the current source.

Fig. 9. Parameter values of lines of different widths. a: $W_{1/3}$, b: MTW, c: $W_{1/2}$, d: $W_{2/3}$.

Fig. 10. The mean value of each parameter as a function of range for tracks of nuclei of charge 6, 12 and 26.
a: $W_{1/3}$, b: MTW, c: $W_{1/2}$, d: $W_{2/3}$.

Fig. 11. The mean value of each parameter transformed into width as a function of range.
a: $W_{1/3}$, b: MTW, c: $W_{1/2}$, d: $W_{2/3}$.
Filled circles: photometer measurements.
Unfilled circles: filar micrometer measurements.

Fig. 12. The charge resolution ΔZ as a function of range for the width parameter $W_{1/2}$. ΔZ has the units of elementary charge.

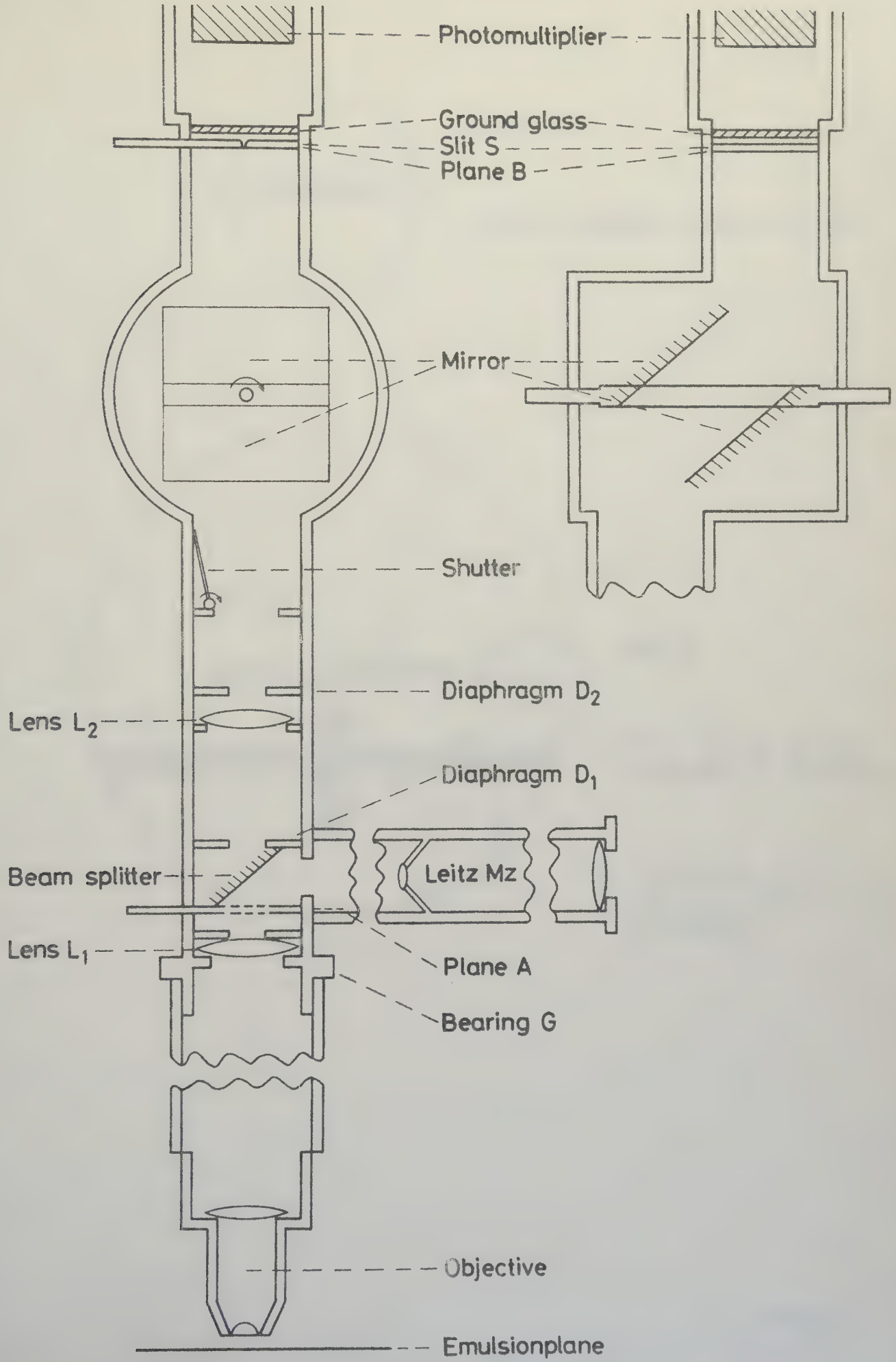
Photomultiplier
Ground glass
Slit S
Plane B
Mirror
Shutter
Diaphragm D_2
Lens L_2
Diaphragm D_1
Beam splitter
Leitz Mz
Lens L_1
Plane A
Bearing G
Objective
Emulsionplane

a

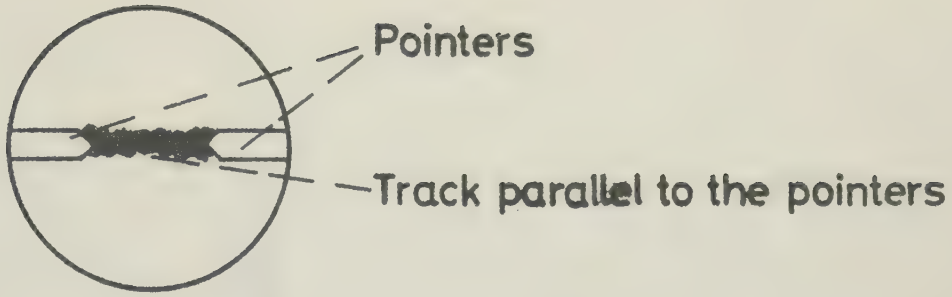
Pointers
Track parallel to the pointers

b

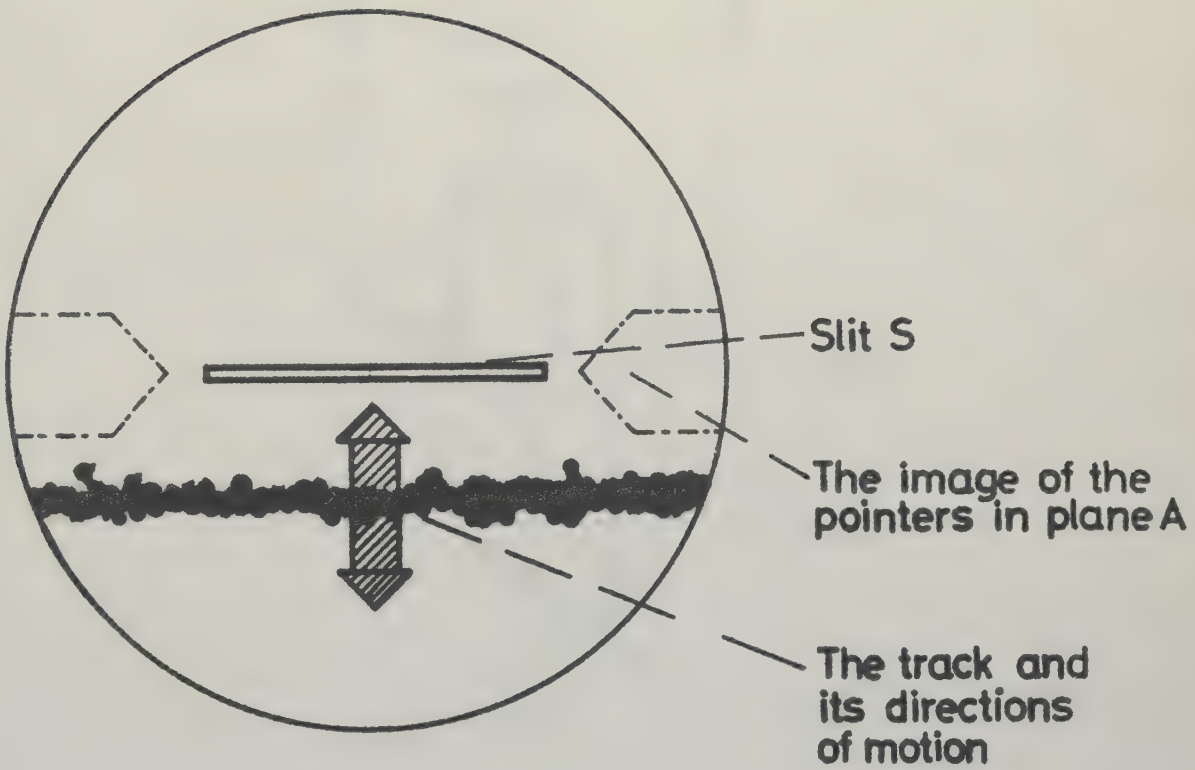
Slit S
The image of the pointers in plane A
The track and its directions of motion

Fig. 2

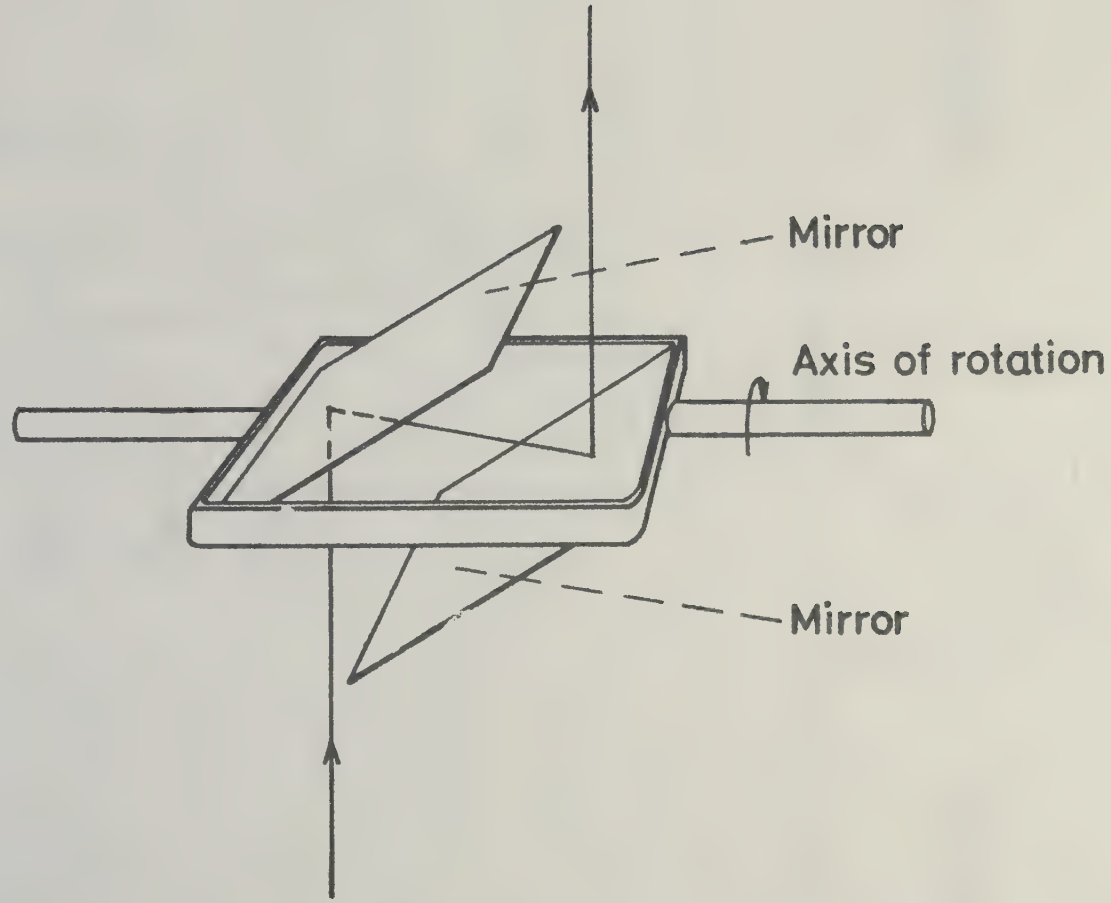

Fig.3

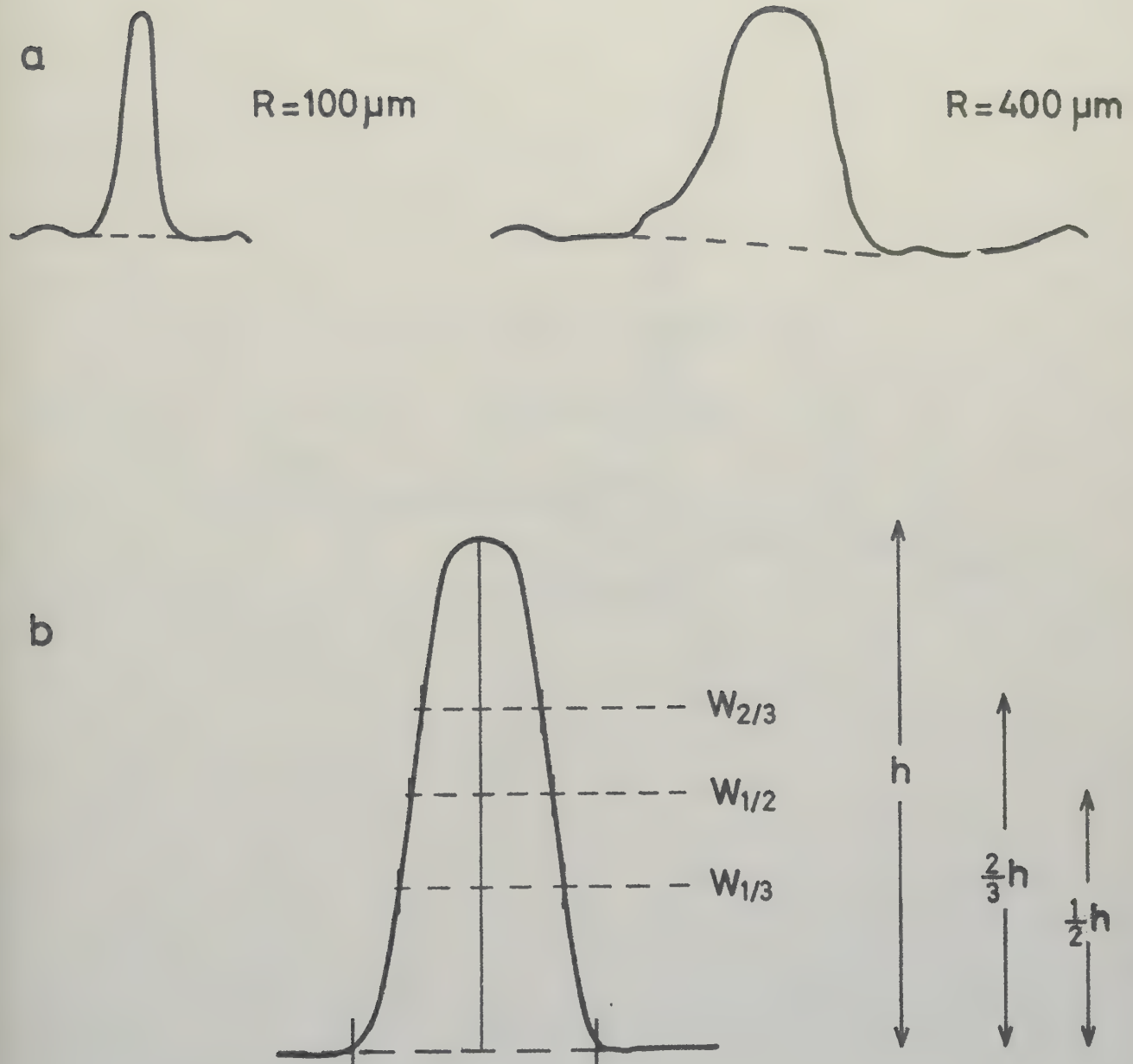

Fig. 4

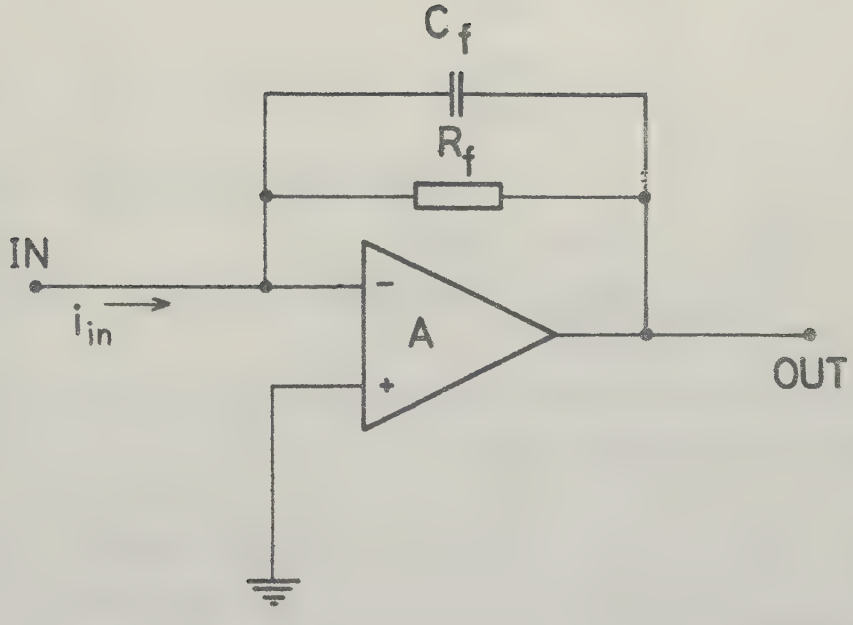

Fig.5

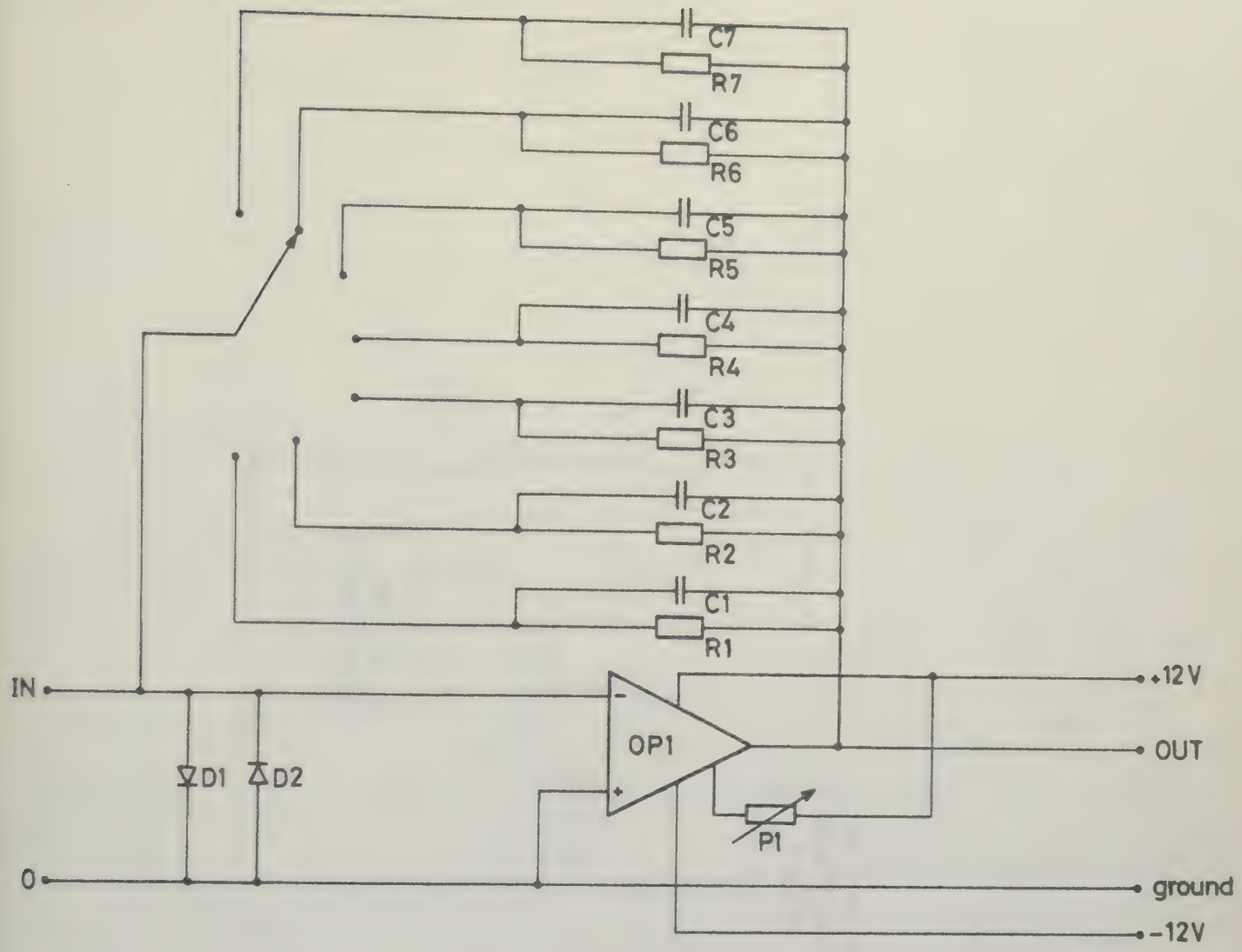

OP 1	1009	Teledyne Philbrick	C 1	3.3 µF	Tantal
D 1, D 2	IN 914	Texas instr	C 2	1.5 µF	-"-
P 1	1 k	Calvern 10 turns	C 3	0.33 µF	Polyester
R 1	1 k	Metal film,0.5%	C 4	0.033 µF	-"-
R 2	5 k	-"- "	C 5	0.033 µF	-"-
R 3	10 k	-"- "	C 6	1.8 nF	-"-
R 4	50 k	-"- "	C 7	1.8 nF	-"-
R 5	100 k	-"- "	Power supply DA 20 Scandia Metric		
R 6	500 k	-"- "			
R 7	1 M	-"- "			

Fig.6

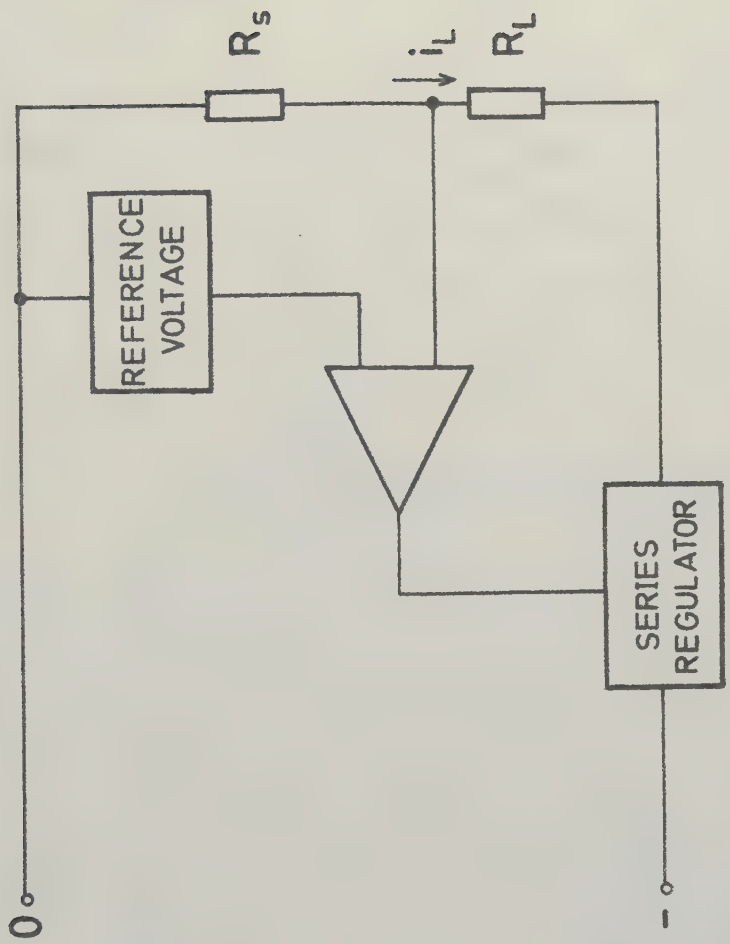

Fig.7

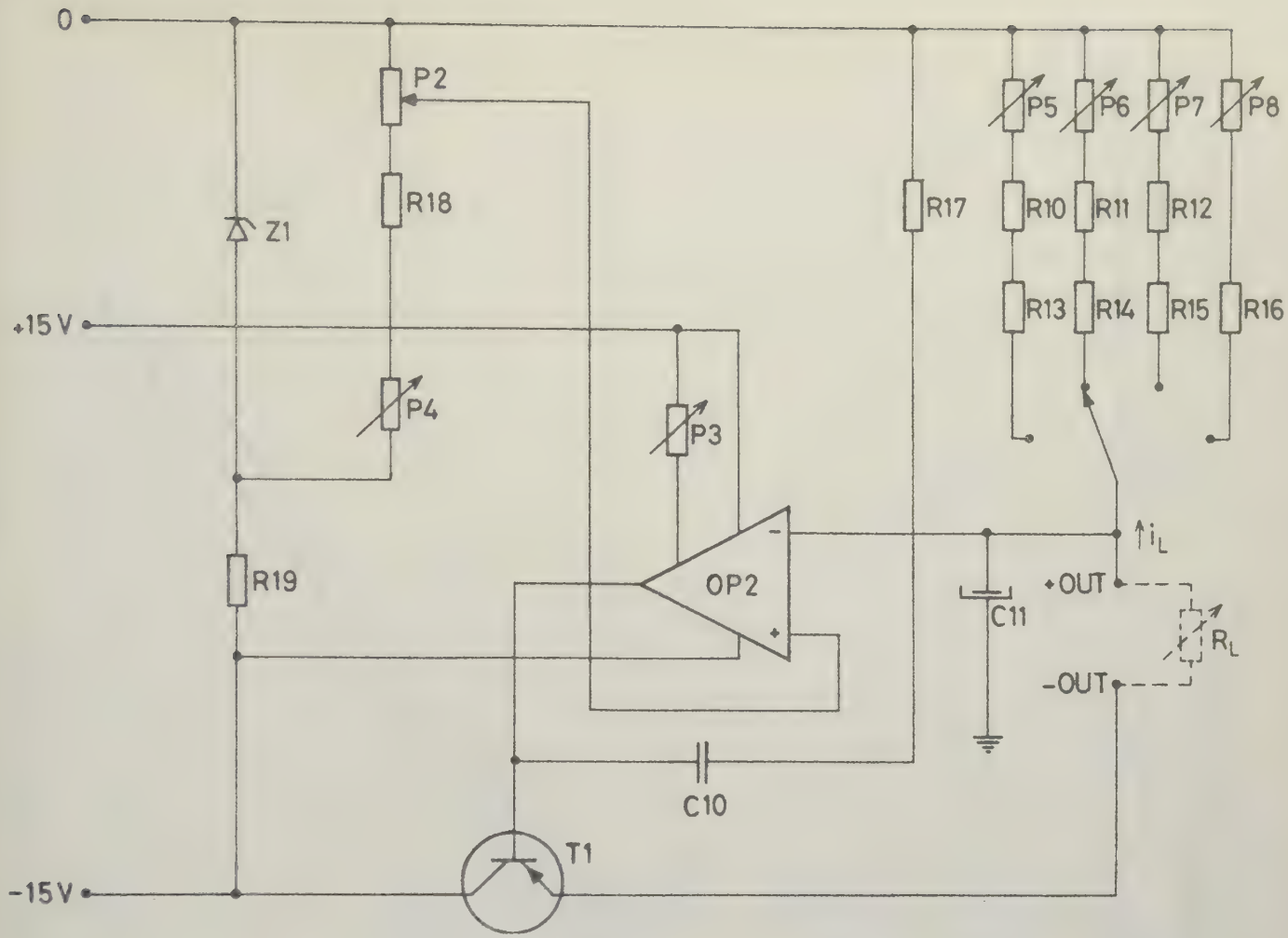

OP 2	1009 Teledyne Philbrick		R 10	10 k	Metal film,1/4 W,1%
T 1	BC 320 Motorola		R 11	100 k	-"-
Z 1	IN 823 Reference diod IR		R 12	1 M	-"-
P 2	100 k Precision potentiometer, lin 0.25%		R 13	2 k	-"-
P 3	1 k Potentiometer wirewound		R 14	20 k	-"-
P 4	100 k -"-	-"-	R 15	200 k	-"-
P 5	1 k -"-	-"-	R 16	1 k	-"-
P 6	10 k -"-	-"-	R 17	2.7 k	Carbon,1/4 W,5%
P 7	20 k -"-	-"-	R 18	330 k	Metal film,1/4 W,1%
P 8	1 k -"-	-"-	R 19	820	Carbon,1/4 W,5%
			C 10	1.3 uF	Polyester 20%
			C 11	10 uF	Electrolytic

Fig.8

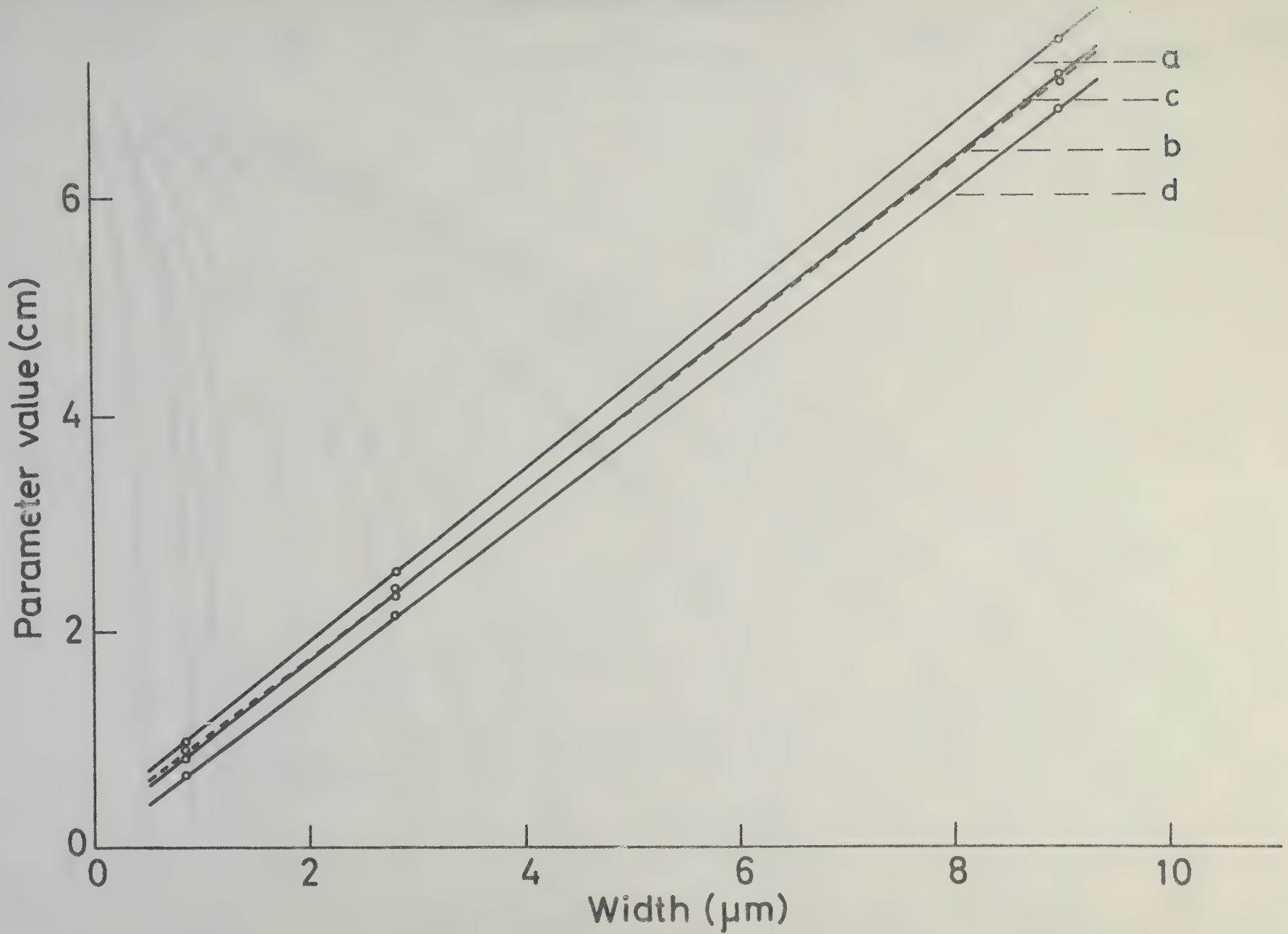

Fig. 9

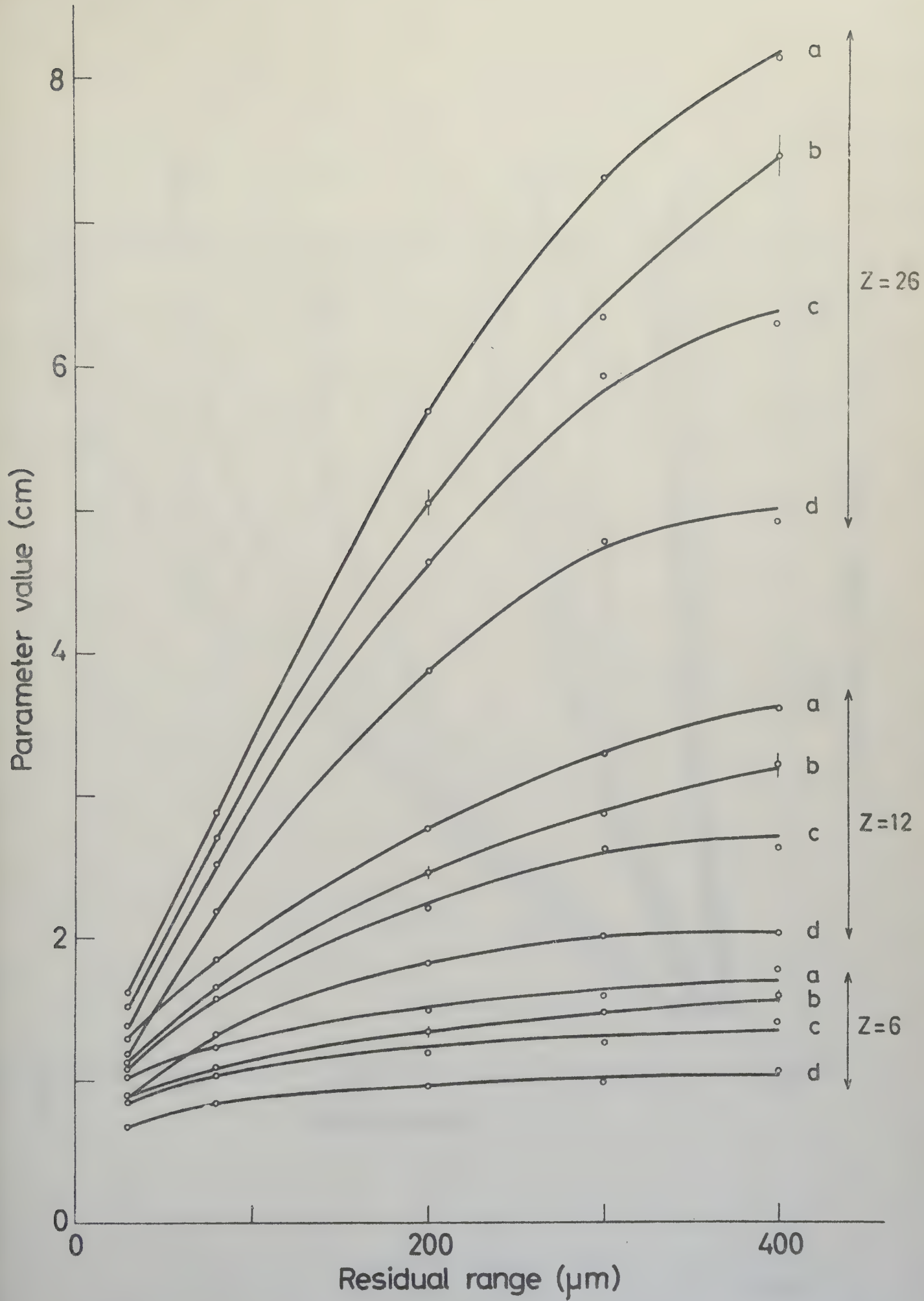
Parameter value (cm)
Residual range (μm)
0
2
4
6
8
0
200
400
a
b
c
d
Z = 26
a
b
c
d
Z = 12
a
b
c
d
Z = 6

Fig. 10

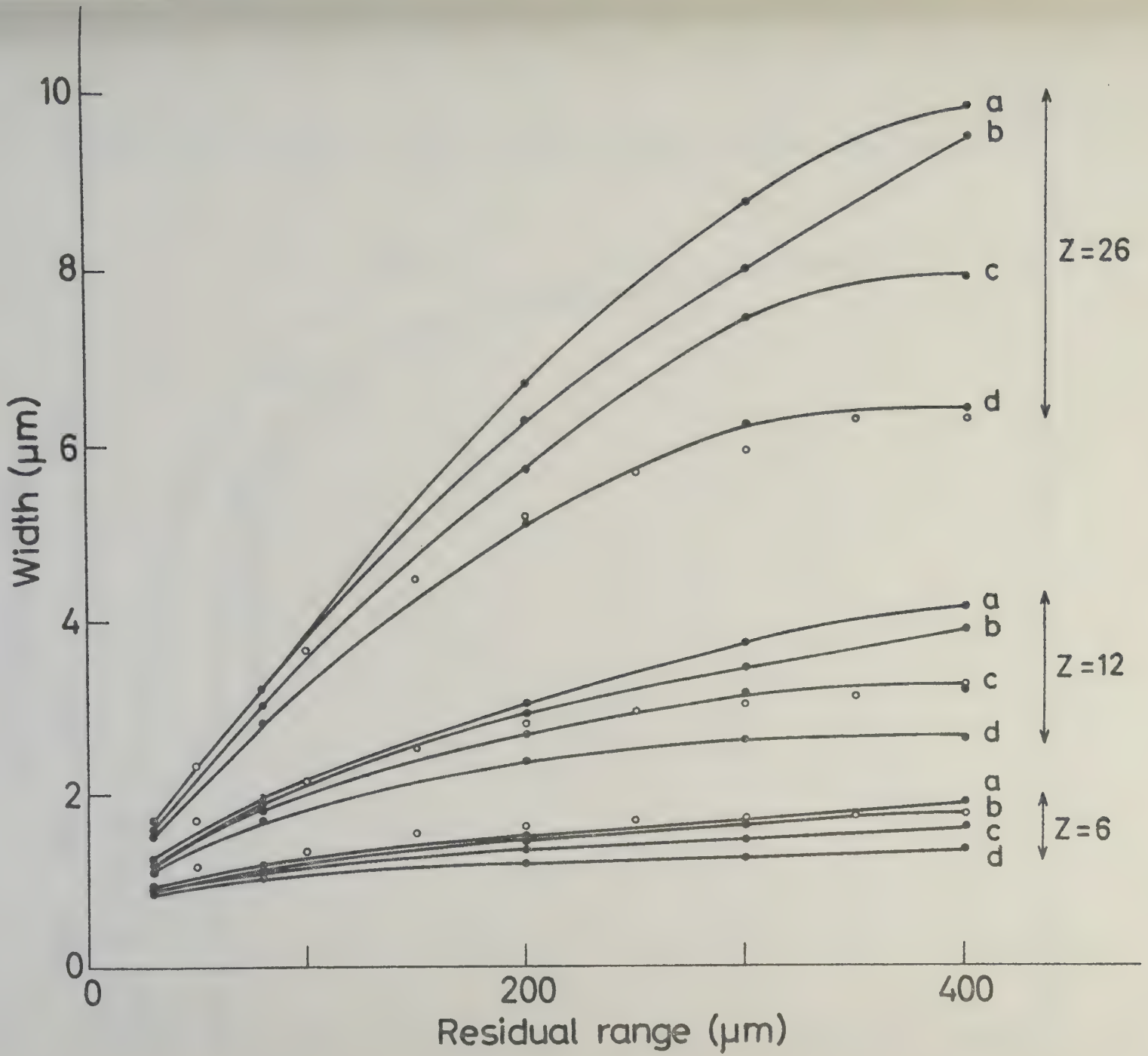
Width (μm)
Residual range (μm)
0
2
4
6
8
10
0
200
400
a
b
c
d
Z=26
a
b
c
d
Z=12
a
b
c
d
Z=6

Fig. 11

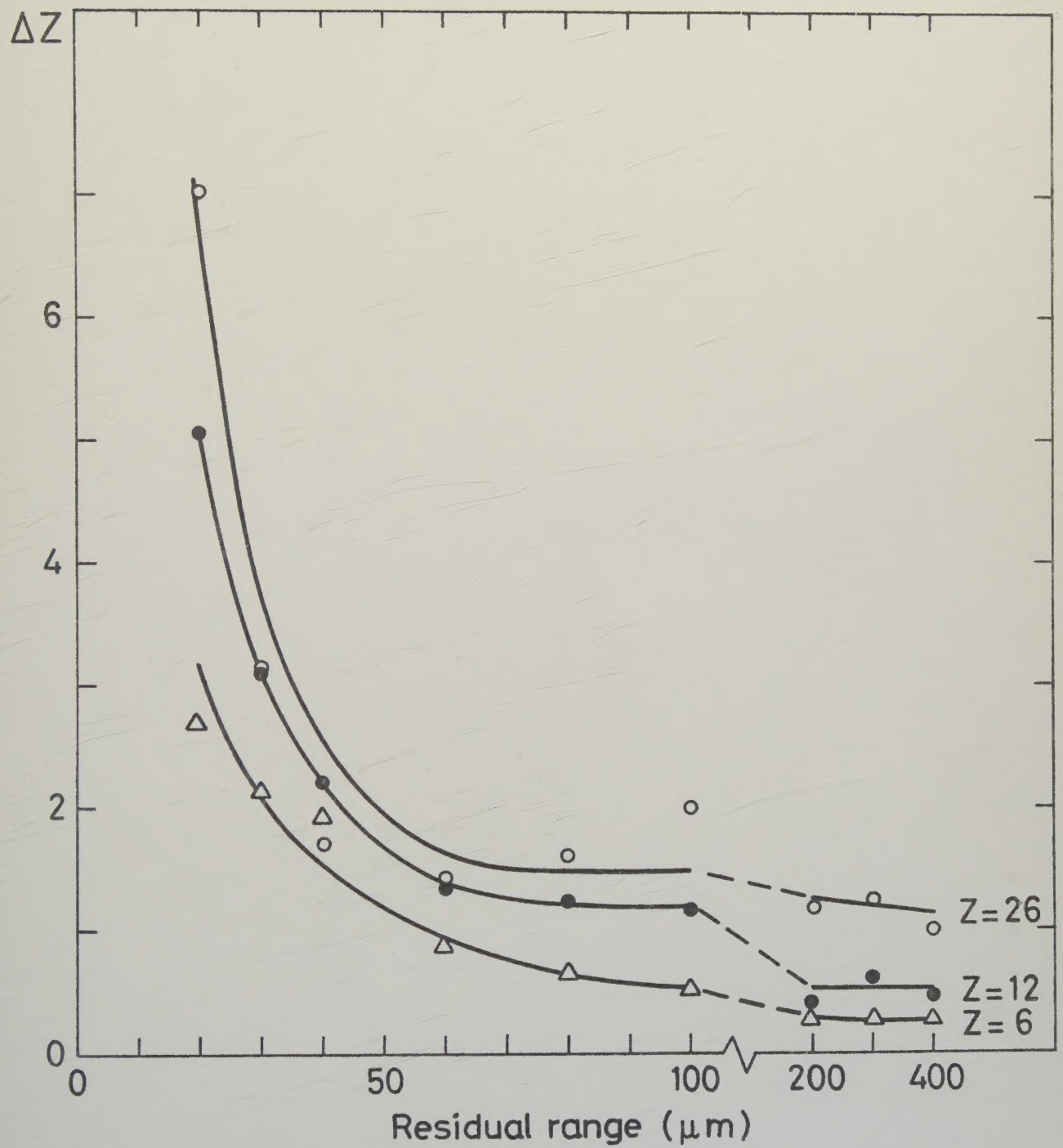

Fig. 12

ΔZ
6
4
2
0
0
50
100
200
400
Residual range (μm)
Z=25
Z=12
Z=6